NATURE AND ORIGIN OF OIKOCRYSTS

IN THE MEGUMA GROUP GOLD DISTRICTS, NOVA SCOTIA

Krista Sutton

Submitted in Partial Fulfillment of the Requirements
for the Degree of Bachelor of Sciences, Honours
Department of Earth Sciences
Dalhousie University, Halifax, Nova Scotia
April 2007

Dalhousie University

Department of Earth Sciences
Halifax, Nova Scotia
Canada B3H 3J5
(902) 494-2358
FAX (902) 494-6889

DATE: _April 10 2007_

AUTHOR: _Krista Sutton_

TITLE: _Nature and Origin of Oikocrysts in the Meguma Group Gold Districts, Nova Scotia_

Degree: _B. Sc_   Convocation: _May 28_   Year: _2007_

Permission is herewith granted to Dalhousie University to circulate and to have copied for non-commercial purposes, at its discretion, the above title upon the request of individuals or institutions.

_____
Signature of Author

Abstract

Oikocrysts are one of the most enigmatic features of the Meguma Gold districts. They are ovoid aggregates of quartz, carbonate, and sheet silicates, locally associated with sulphide, that commonly define a prominent down-dip lineation on the limbs of gold-bearing anticlines in the central part of the Meguma Group. Regional mapping of the Oldham and Montague gold districts, and sampling at Mooseland, North Brookfield and Caribou, has shown that oikocrysts are confined to the gold districts. A detailed mineralogical and textural investigation of oikocrysts from these areas has been undertaken in an attempt to determine their origin and their link to the gold districts. Oikocrysts occur mainly in slate horizons interlayered with quartzo-feldspathic metasiltstones and metasandstones of the Goldenville Formation. Field observations confirm that the long axes of the elongated oikocrysts define down-dip lineations on cleavage planes perpendicular to anticlinal fold hinges. Although in hand sample they resemble deformed porphyroblasts, internal mineralogy and texture are not consistent with this interpretation. Instead, their internal features resemble the mineralogy and texture of interlayered metasiltstones. In some cases, an apparent progression from cusps of deformed metasiltstone layers at slate boundaries to isolated oikocrysts in the adjacent slate can be observed. These features point to the possibility that oikocrysts are microlithons of highly deformed metasiltstone layers. The analysis of sulphide minerals under reflected light reveals that arsenopyrite is coarse-grained and idioblastic while other sulphides are fine-grained with irregular grain boundaries, possibly linking sulphide volume loss to oikocrysts. Oikocryst aspect ratios (4:1 to 12:1) reflect the amount of strain in the slate, which is interpreted to reflect folding. The relative age of oikocryst formation can be constrained by cross-cutting relationships. The quartz-rich aggregates pre-date or are synchronous with at least one stage of cleavage formation, although it is likely that the biotite-chlorite rims formed later. The oikocrysts and their rims pre-date at least one generation of quartz veins and in the Mooseland district they appear to pre-date contact metamorphism. Overall these observations suggest that the interior aggregate formed prior to the rim, and have a close relationship to sulphide minerals and microlithon domains.

Keywords: Goldenville Formation, lineation, microlithon, petrology, mineral aggregate, sulphides, gold districts

TABLE OF CONTENTS

List of Tables and Figures   **Page**

Acknowledgements

I would like to thank many people for their contributions to this thesis. I would like to thank the whole Earth Sciences Department at Dalhousie University for their support over the last four years and the Nova Scotia Department of Natural Resources for aid in funding this project. I would also like to thank my family, my friends, and Sam for their unrelenting encouragement and support throughout the year. Lastly, my most sincere thanks go to my supervisors Rick Horne and Dr. Rebecca Jamieson for their enthusiasm, guidance, and encouragement for the duration of the writing of this thesis.

Chapter 1

INTRODUCTION

1.1 Opening Statement

The origin of the Meguma Group gold deposits has been of interest since gold was first discovered in the late 1800's (Bates, 1987). The understanding of the deposits and associated alteration and deformation features has evolved over time as more data have been acquired. There is, however, a feature of some Meguma gold districts that remains poorly understood. Many gold districts in the Meguma Group feature a distinct lineation defined by cigar-shaped mineral aggregates in the metasiltstone intervals, referred to as "oikocrysts" (Kontak and Smith, 1990). This thesis will attempt to explain their origin, timing, and relationship to strain and gold mineralization; through petrographic and microprobe analysis of oikocryst samples from selected Meguma Group gold districts.

1.2 Geological Setting of Meguma Gold Districts

The Cambrian to Ordovician Meguma Group consists of two main units, the lower, metasandstone-dominated Goldenville Formation and the upper, slate-dominated Halifax Formation. The Nova Scotia Department of Natural Resources has recently proposed elevating the Meguma Group to the Meguma Supergroup, but older terminology is retained here for consistency with most published literature (White, 2007). The Goldenville Formation is understood to be a turbiditic, deep-sea fan complex. The rocks were affected by greenschist to amphibolite facies regional metamorphism (ca 400-390 Ma) that was locally overprinted by contact metamorphism associated with intrusion of

the 380 Ma South Mountain Batholith and associated plutons. Regional metamorphism is thought to have been synchronous with regional folding. This is discussed further in section 1.4.

The gold districts are structurally set in the dominant, gently plunging, upright, sub-horizontal, NE-SW trending regional folds, with an observed axial planar fanned cleavage (Smith and Kontak, 1996; Keppie et al., 2002). The steep and overturned limbs near the hinge zones of anticlines host the gold deposits. Quartz veins in the anticlines were emplaced by hydro-fracturing in areas of brittle-ductile deformation (Smith and Kontak, 1996). The most prominent and richest veins are parallel to bedding, forming saddle reef structures in the hinges of antiforms (Smith and Kontak, 1988). Other veins include discordant, en echelon, stockwork, fissure veins and a-c veins (Smith and Kontak, 1996). High-grade (<15 g/t Au) ore is common at the intersection of angular or fissure veins with the bedding-concordant veins (Smith and Kontak, 1996). Many of the vein systems extend laterally for kilometers (Smith and Kontak, 1996). The mineralogy of the veins is dominated by quartz, carbonate, and Fe-sulphides, including native gold (Kontak et al., 1990). The native gold ranges from nugget size to micron scale sized grains (Smith and Kontak, 1996).

The biotite in the auriferous veins in the fold hinges have an age of 370 ± 8 Ma and the fold terminations, like the northeastern termination of the Oldham anticline, represent the youngest increment of folding (Keppie et al., 2002). The vertical stretching component of deformation, which is associated with oikocrysts, is unknown; however the whole rock ages were dated to be 378-366 Ma using $^{40}Ar/^{39}Ar$ dating. This implies that

the vein fluids moved into the conical fold terminations as they formed (Keppie et al. 2002).

The mechanisms proposed for the genesis of gold mineralization include epigenetic emplacement related to granitic plutonism (MacDonald and OReilly, 1989), and vein emplacement along late shear zones (Henderson and Henderson, 1986). Multiple source reservoirs have been proposed, including the Meguma Group and its underlying basement, for the auriferous carbonate-rich fluids (Smith and Kontak, 1996).

For this thesis, the focus is on the nature of the vertical stretching component of deformation in this tectonothermal system (Keppie et al., 2002) which is linked to the evolution of oikocrysts. Oikocryst samples were taken from the Oldham, Montague, Caribou, North Brookfield and Mooseland districts, which are primarily situated in the Goldenville Formation (Fig 1.1).

1.3 Previous Work on Oikocrysts

The earliest recognition of oikocrysts in the Meguma terrane is not recorded; however their abundance in the metasiltstone and slate of the Goldenville Formation in gold districts suggests that early prospectors would have noticed them. There is no documented occurrence of gold-deposit associated oikocrysts anywhere else in the world. They were initially regarded as mineral lineations (Melvin, 1987) but with closer analysis they were recognized as biotite-rich aggregates (MacDonald, 1998). Kontak and Smith (1990) first described them as oikocrysts. Oikocrysts are defined as "a matrix or host crystal through which smaller crystals (chadacrysts) of other minerals are distributed as poikilitic inclusions" (American Geological Institute, 1960).
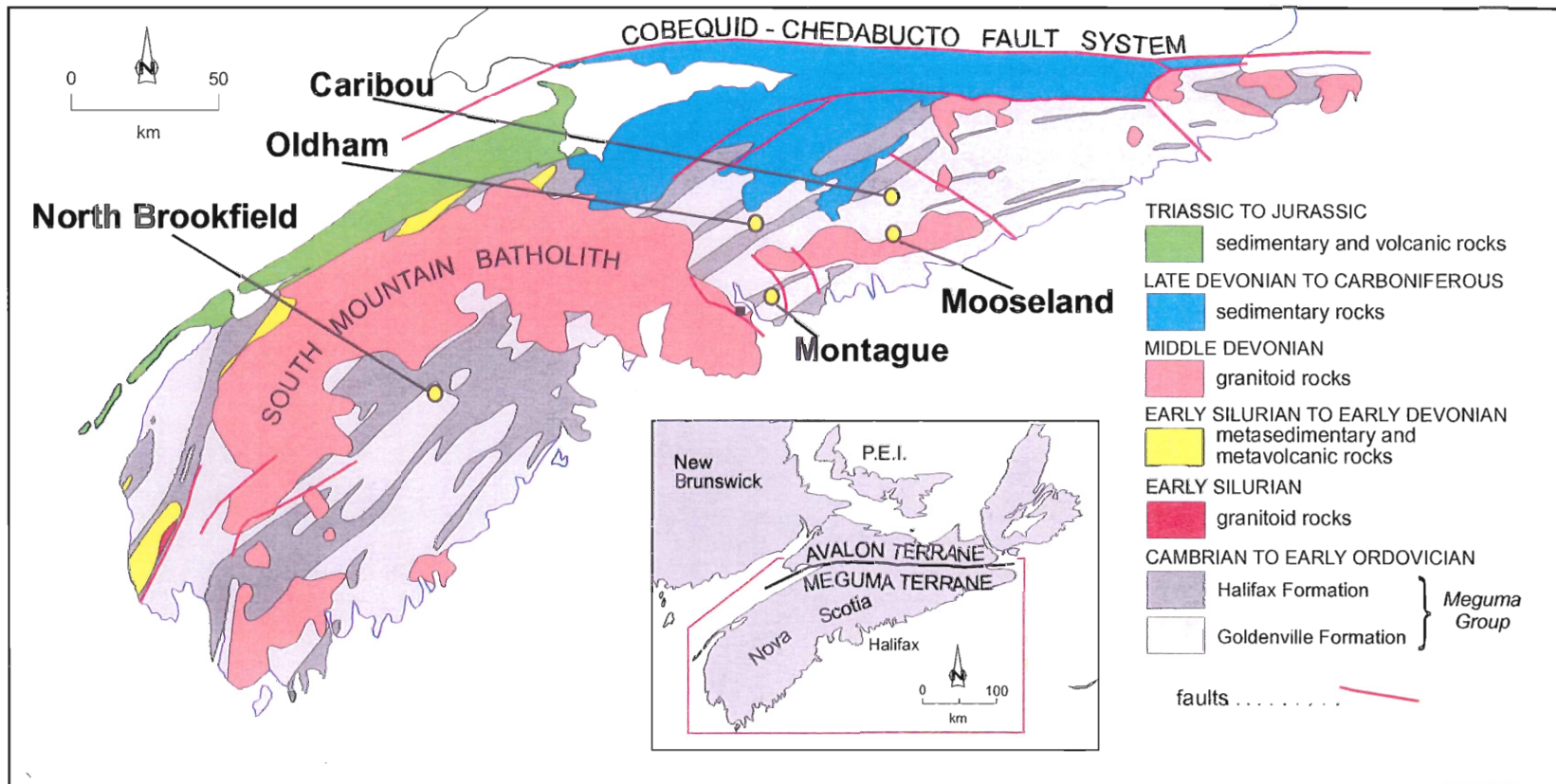
Figure 1.1 Geological map of Nova Scotia displaying the gold districts (yellow circles) visited for this study, all within the Meguma Group, Halifax and Goldenville Formations.

In the study area, oikocrysts are ellipsoidal or cigar-shaped aggregates with cores consisting of granular quartz, chlorite with traces of carbonate and other minerals, and typically rimmed by biotite-chlorite intergrowths. They are coarser-grained than the slate matrix and have a polygonal internal texture. It has also been observed that the foliated matrix is deflected around the oikocrysts (MacDonald, 1998).

The structure of oikocrysts is of great interest. Their long axes form down-dip lineations on the cleavage planes oriented perpendicular to the fold hinge (intersection lineation) and parallel to the matrix foliation (Horne et al., 1996). This lineation is related to the vertical stretching during regional folding and it has been observed that the amount of elongation of the long axes of oikocrysts varies systematically with the amount of vertical stretching.

A two-stage model for oikocryst formation was proposed by Horne et al. (1996). The first stage was the development of equant oikocrysts and the emplacement of veins, followed by strain and regional folding. There is a possible genetic link between vein and oikocryst emplacement since they are both restricted to auriferous veined districts. This leads to the hypothesis that they formed in response to hydrothermal fluid flow and are a product of a metasomatic reaction, rather than a feature that originated from regional or contact metamorphism (Horne et al. 1996). Secondly, late-stage regional folding and shearing, parallel to bedding resulted in the elongation of oikocrysts and the folding of quartz veins. Their spatial relationship to auriferous veins may make them a valuable exploration tool (Horne et al. 1996).

1.4 Regional Metamorphism

The turbiditic metasandstone and slate of the Goldenville Formation and the overlying Halifax Formation slates were deformed and metamorphosed during the Early to Late Devonian Acadian Orogeny (Hicks, 1996 and references therein). Regional deformation caused buckling of the competent quartz veins (Fig. 1.2), a uniform slaty cleavage, and tight chevron folds ranging from the centimeter to the kilometer scale (Hicks, 1996). The regional-scale folds are northeast-trending with a well developed axial planar slaty cleavage (White, 2003). This cleavage is well developed throughout the slate horizons in all the gold districts. Cleavage measurements were collected at outcrops in the gold districts that were considered to be dominated by early structures and that would represent regional folding. Cleavage is formed by contraction in a direction perpendicular to the plane of cleavage and extension in the direction of cleavage dip (Wood, 1974). Cleavage forms via a combination of mechanical and chemical processes including ductile deformation and diffusive mass transfer. (Wood, 1974). At Oldham the cleavage strikes between 240° and 250°. At Montague cleavage strikes approximately 060°. The cleavage dips average between 75° and vertical. The variation is caused by later, smaller-scale strain.

Based on $^{40}Ar/^{39}Ar$ ages from single muscovite grains and whole-rock samples from the Meguma Group, the timing of regional metamorphism occurred between 388-406 Ma (White, 2003). Regional metamorphism of the Meguma Group grades from greenschist facies in the west to amphibolite facies in the east (Keppie and Muecke, 1979). Some areas are locally in sub-greenschist facies, where rocks retain their original sedimentary structures and detrital muscovite ages (Hicks, 1996). The Oldham district is within the biotite metamorphic zone. Caribou, North Brookfield, Montague and

Mooseland are in the chlorite metamorphic zone. Mooseland and Montague are in the

biotite zone of contact metamorphism where biotite overprints the regional metamorphic

mineral assemblages and defines a late schistosity (S_2) (chapter 3). North Brookfield lies

within the cordierite zone of contact metamorphism because of its proximity to the SMB,

therefore it has cordierite overprinting its regional metamorphic mineral assemblage

(Chapter 4).

Figure 1.2: Station O-4 on the Wallace Lead, Oldham district. Open cut trench exposing a
buckled weathered quartz vein between upper metasandstone bed and lower cleaved slates
and shales. Red indicates location and shape of bucked vein. Shallow angle of bedding (S_o) is
due to proximity to fold hinge.

1.4 Statement of Problems and Objectives

Based on their petrographic and structural features and spatial association with gold

districts, three hypotheses will be evaluated in order to explain the origin of oikocrysts.

1) Oikocrysts are altered remnants of porphyroblasts (probably cordierite) formed

during regional or contact metamorphism. Cordierite is associated with

metamorphism of the Meguma Group and in thin section closely resembles oikocrysts in size and shape (Kontak and Smith, 1990).

2) Oikocrysts are replacement products after arsenopyrite or other Fe-sulphides. Where Fe-sulphides are present in the rocks, they are porphyroblasts of arsenopyrite within the cores of oikocrysts, with inclusions of pyrrhotite, chalcopyrite and pyrite. In rocks where arsenopyrite does not dominate as porphyroblasts, remnant grains of Fe-sulphides exist in some oikocrysts.

3) Oikocrysts are isolated fragments or microlithons of highly deformed metasiltstone layers. A moderately rough disjunctive foliation may have caused the isolation of oikocrysts in the matrix during vertical stretching. Cusp and lobe structures on metasiltstone-slate contacts provide evidence for this.

The primary objective of this thesis is to test these hypotheses and to explain the origin of oikocrysts. The short-term objectives are to document their distribution in the field, describe their mineralogy and texture using thin section and microprobe analysis, and to determine their age relative to fabrics, veins, contact metamorphism and other features.

Chapter 2

FIELD RELATIONSHIPS

2.1 Introduction

There are many Meguma Group gold districts that host oikocrysts. Through field research and documentation at various locations over the past century, it was understood that oikocrysts were not just a ubiquitous feature of the Meguma Group, but linked in some way to fold geometry in the gold districts, and possibly to regional deformation and/or contact metamorphism. The form of metamorphism causing the oikocrysts is less clear than the geometrical relationship to folds. Some have hypothesized (Kontak and Smith, 1990) that they may be related to regional metamorphism; however their limited distribution suggests a genetic link to gold mineralization. Field work completed for this thesis focused on systematic sampling in certain gold districts in order to document their geometrical relationship to folds and to other features, including metamorphism and distribution of gold veins.

2.2 Sample Collection and Location

Field work was conducted over three non-consecutive days in September and October 2006. The days were spent at locations that provided the greatest opportunity for finding outcrop with good oikocryst exposure for sampling and data collection. However, back-filling of open shafts and trenches and abundant vegetation overgrowth at the old mine sites hindered access to good outcrop. This has limited my ability to quantify the distribution of oikocrysts in outcrop within and between districts. This thesis is therefore a preliminary, qualitative representation of the oikocrysts in relation to

structures. To supplement outcrop data, loose waste-rock at many locations near old mine workings was sampled, assuming it to be from the nearest shafts.

Samples were collected at the Mooseland, North Brookfield and Caribou districts and more extensively at the Oldham (Fig. 2.1) and Montague (Fig. 2.2) districts where their locations were referenced through Global Positioning Systems and air-photo mapping.

2.2.1 Oldham district samples

The Oldham anticline outcrops in the Goldenville Formation as a NE-SW trending folds that extends from the Shubenacadie Lake to 3 km northeast of the town of Oldham (Keppie et al., 2002). After detailed mapping by Faribault (1898) during active mining, it was determined that the Oldham anticline terminates in two conical folds (Keppie et al., 2002). Active mining took place between 1862 and 1938, and produced 85,295 ounces of gold (NSDNR, 2007). The Oldham deposit mine workings were made up of various north-south trending trenches that varied in depth and width. Some of the deepest mine shafts in Nova Scotia were excavated at Oldham; however they were later filled in for safety reasons. For this study, outcrop was found in trenches and near old mine shafts where clearing took place, and also under uprooted trees. Various observations were taken at these locations. At Oldham loose samples were collected showing slate and metasiltstone layers with oikocrysts that vary in concentration and shape with lithology (Fig. 2.3 and Fig. 2.4), as well as samples containing kink-bands, sulphide porphyroblasts, and quartz stringers. Samples that may reveal age relationships were sought. Oikocrysts were rounder in the metasiltstone horizons near the hinge of the fold. The samples with sulphide porphyroblasts

Legend:
- ∧ Oldham Sample Locations
- — ╪ - Anticline/ Syncline
- ● Shafts
- — Veins
- — — Faults
- Swamps
- Roads
- Streams/Lakes
- Buildings

Inset map labels: New Brunswick, P.E.I., AVALON TERRANE, MEGUMA TERRANE, Nova Scotia, Halifax, 0 — 100 km

Sample locations: OLD 1, OLD 2, OLD 3, OLD 4, OLD 5, OLD 6, OLD 7, OLD 8, OLD 9, OLD 10, OLD 11

Scale: Meters 430 215 0 430
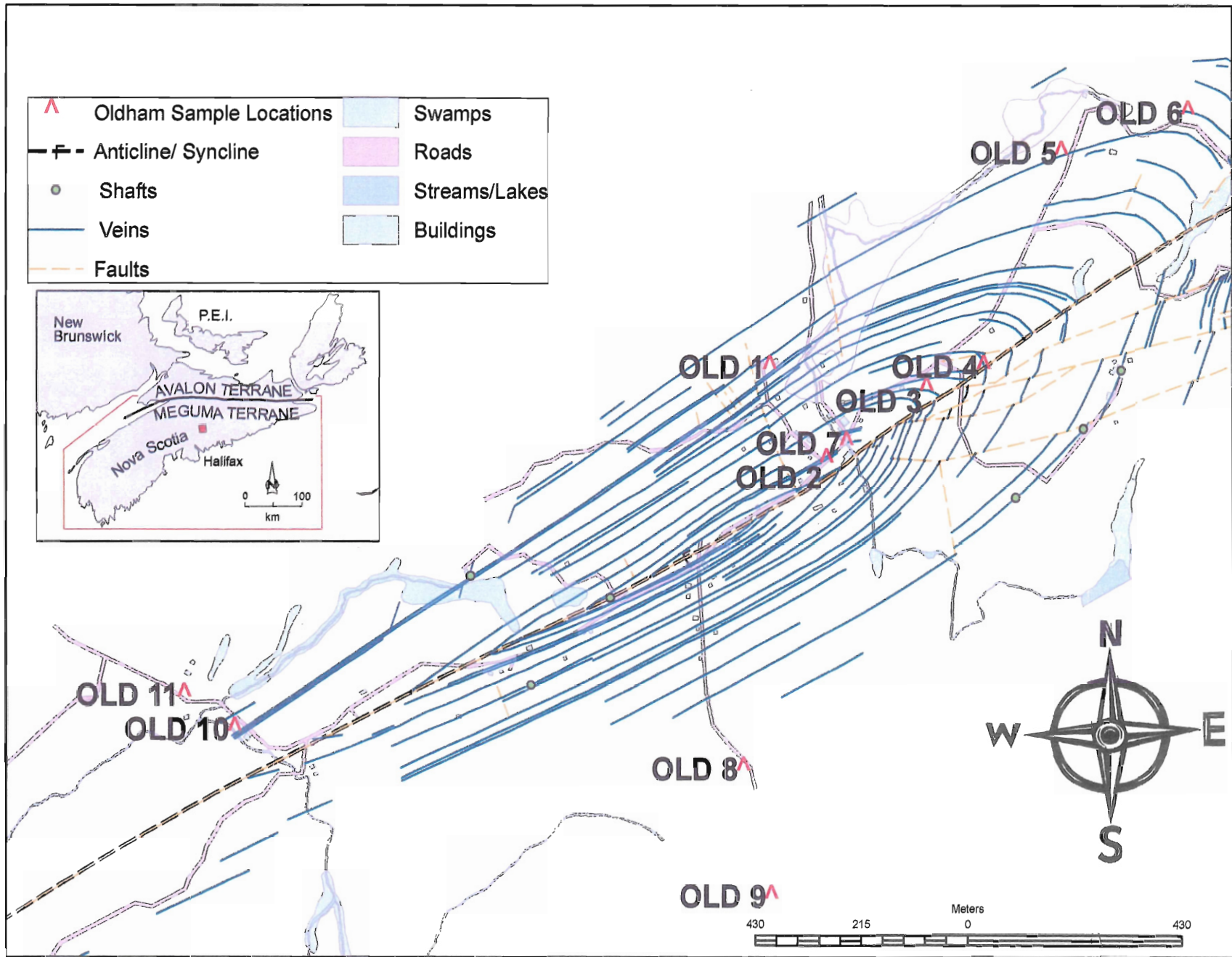
Figure 2.1. Map of the Oldham Gold District showing sample locations. (after Faribault, 1989)
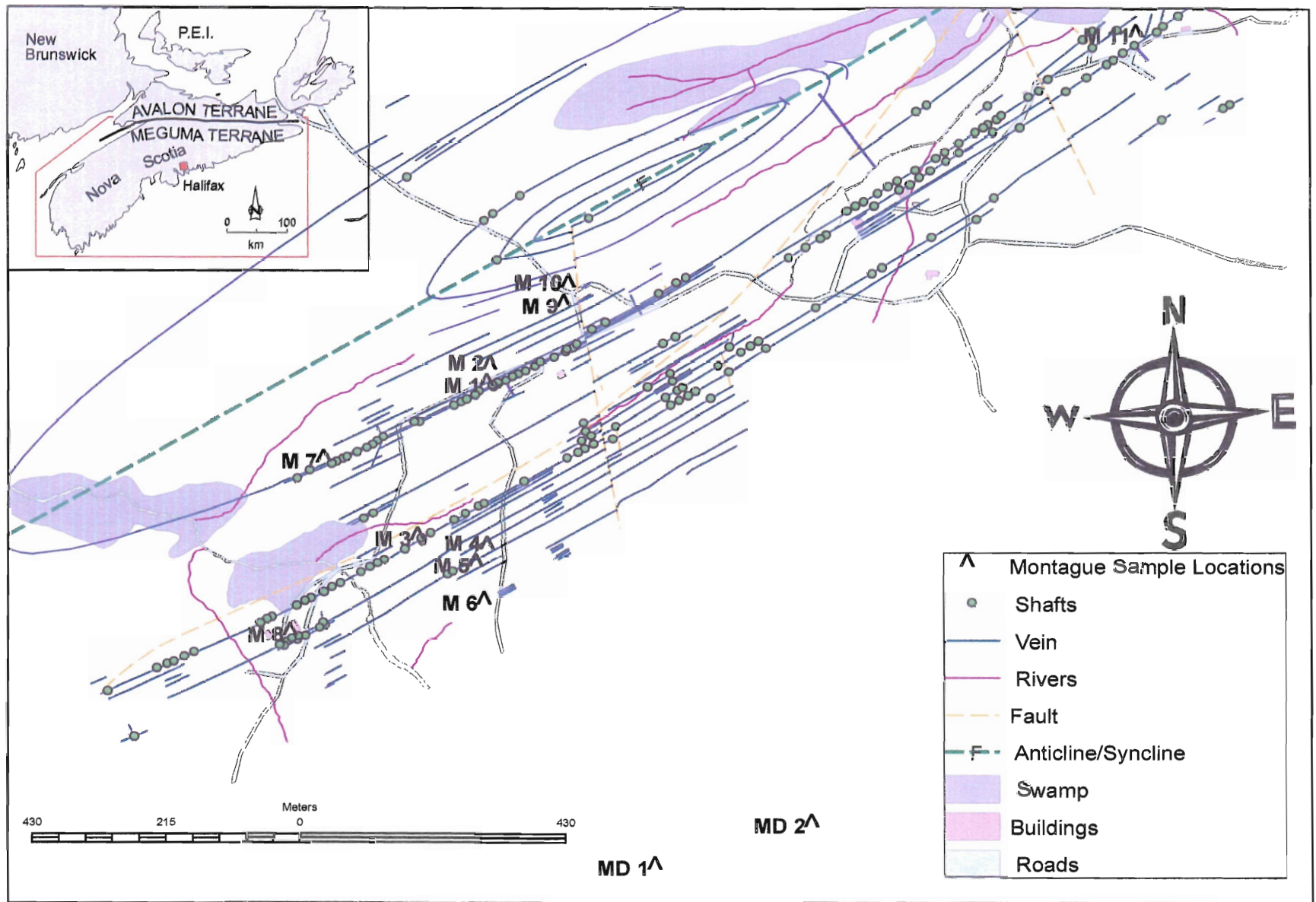
Figure 2.2. Map of the Montague Gold District showing sample locations. Stations MD1 and MD2 are outside the gold district. (after Faribault, 1989)

Figure 2.3: Station M-8 from Montague: A loose sample showing beds with high concentration (black) and low concentration (red) of oikocrysts, corresponding respectively to layers of slate and metasiltstone. (rock hammer for scale)
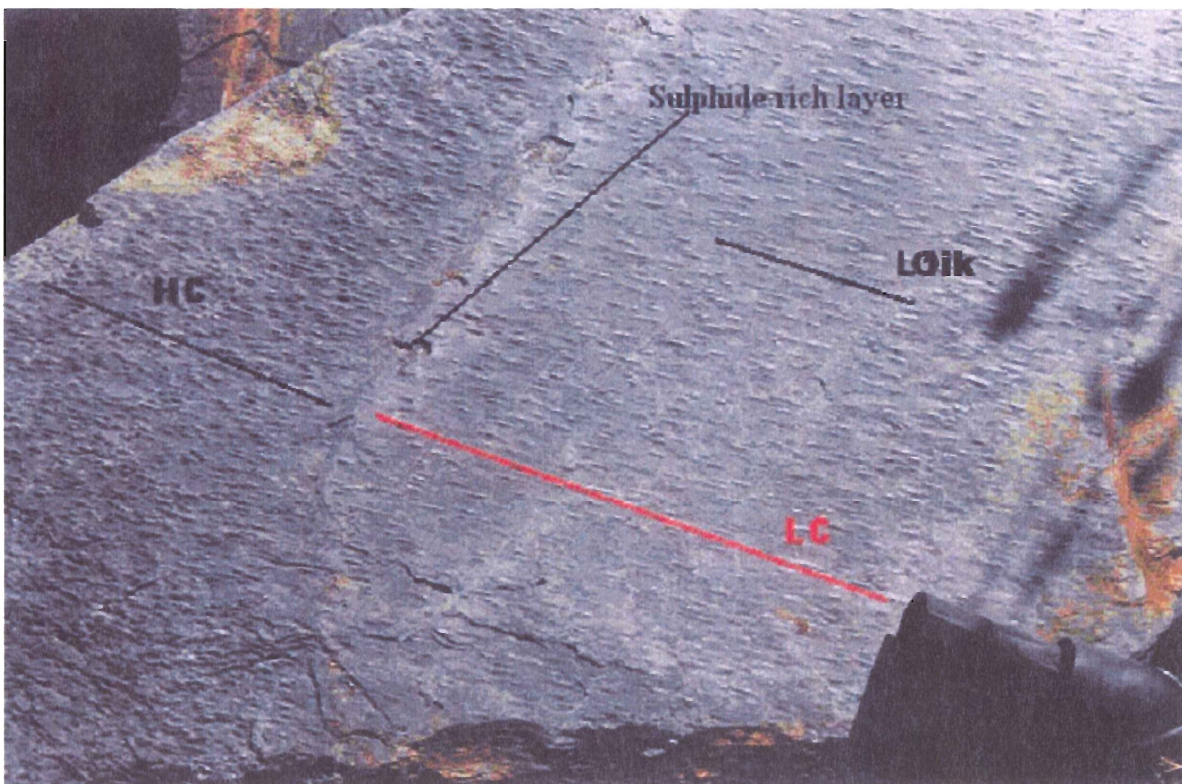
Figure 2.4: Station M-9 from Montague: Loose sample showing oikocryst concentration relative to bedding and lithology, and weathered sulphide-rich bed (marker for scale).
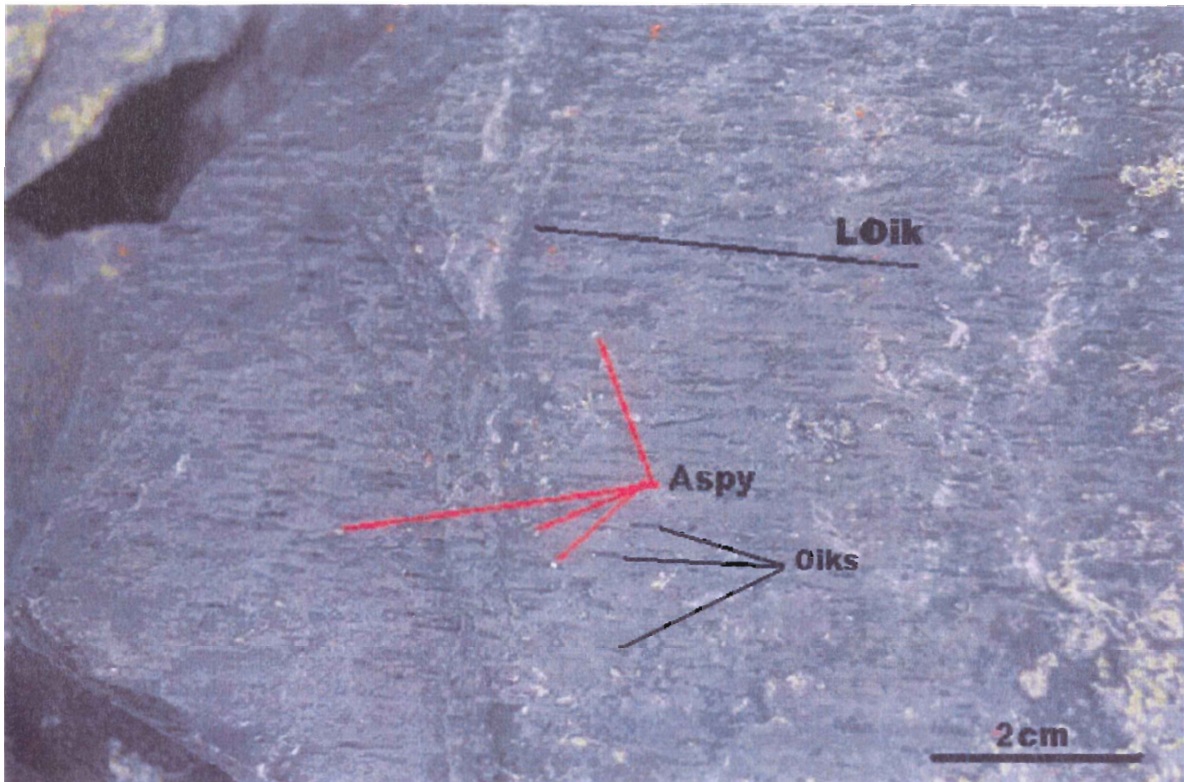
Figure 2.5: Station O-4: A loose sample of oxidized arsenopyrite porphyroblasts within oikocrysts, from outcrop on the Wallace Lead in the Oldham district.

within the oikocrysts, which are located closer to veins, were weathered out (Fig. 2.5). This spotty shape and weathering of the oikocrysts was not observed in the dark slate layers of the main gold leads, like the Blue lead and Mitchell lead named in Faribault's Gold District Map (1898).

A few samples outside the mine site were taken for comparison with lithologies within the district. Sample OLD-9 consists of metasiltstone interbedded with several dark thin slate horizons. The lithology of the rocks resembles those seen within the districts; however no oikocrysts were found on the cleavage planes. Muscovite porphyroblasts were well developed through the outcrop. Sample OLD-10 was located at a cliff on the side of a river, outside of the main mine site, but approximately 200 m along strike from old trenches. It showed the same sequence of rocks as in the district, and oikocrysts were found throughout. Only a few hundred meters down the highway at station OLD-11, the

metasandstone and slate layers lack oikocrysts. This location was outside the gold district and away from the hinge zone.

2.2.2 Montague district samples

The Montague anticline outcrops in the Goldenville Formation as a NE-SW trending fold. It is located northwest of Dartmouth. Montague was in production between 1863 and 1938 and produced 68,139 ounces of gold (NSDNR, 1976). The Montague district mine workings consisted of various shallow and extended open-cut trenches up to 1.4 m wide that followed different leads. Many open shafts were spread out through the districts and were aligned over the various leads. Waste rock material was left on surfaces as ridges or as piles in clearings. Old concrete foundations are scattered throughout the area. The samples at this district were taken from piles and from leads where good outcrop and consistent oikocryst orientation were apparent. Most trenches were trending 60°, or when the folds were overturned the trenches trend 240°. Outcrop samples were taken in order to represent oikocrysts in the various leads and to document any variation between leads and between districts. Some leads varied in oikocryst concentration from east to west. Sample M-9 (Fig. 2.2) contains an 8 cm wide quartz vein in the slate. There are inclusions of bedrock, and abundant arsenopyrite and other sulphides visible in the veins, and oikocrysts are present. Further west along the Iron belt, at the southwest end of the anticline, the oikocrysts are not well developed, even though it is close to a 30 cm wide bedding-parallel quartz vein.

Loose samples were taken from rock piles and showed lithological, sulphide, and quartz veins. Field observations are consistent with those in the Oldham district. Lithology affects the shapes and concentration of oikocrysts. When sulphides are present, they are concentrated in the cores of the oikocrysts.

On the south limb of the Montague anticline, on Montague Drive outside the Montague district, two samples, MD-1 and MD-2, were taken from bedding that was overturned and striking 235° and dipping 80° with a well defined cleavage. The rocks are dark slate and metasandstone that resemble the lithologies within the gold district; however there are no oikocrysts or even weathered sulphide spots in either of the beds (Fig. 2.6).
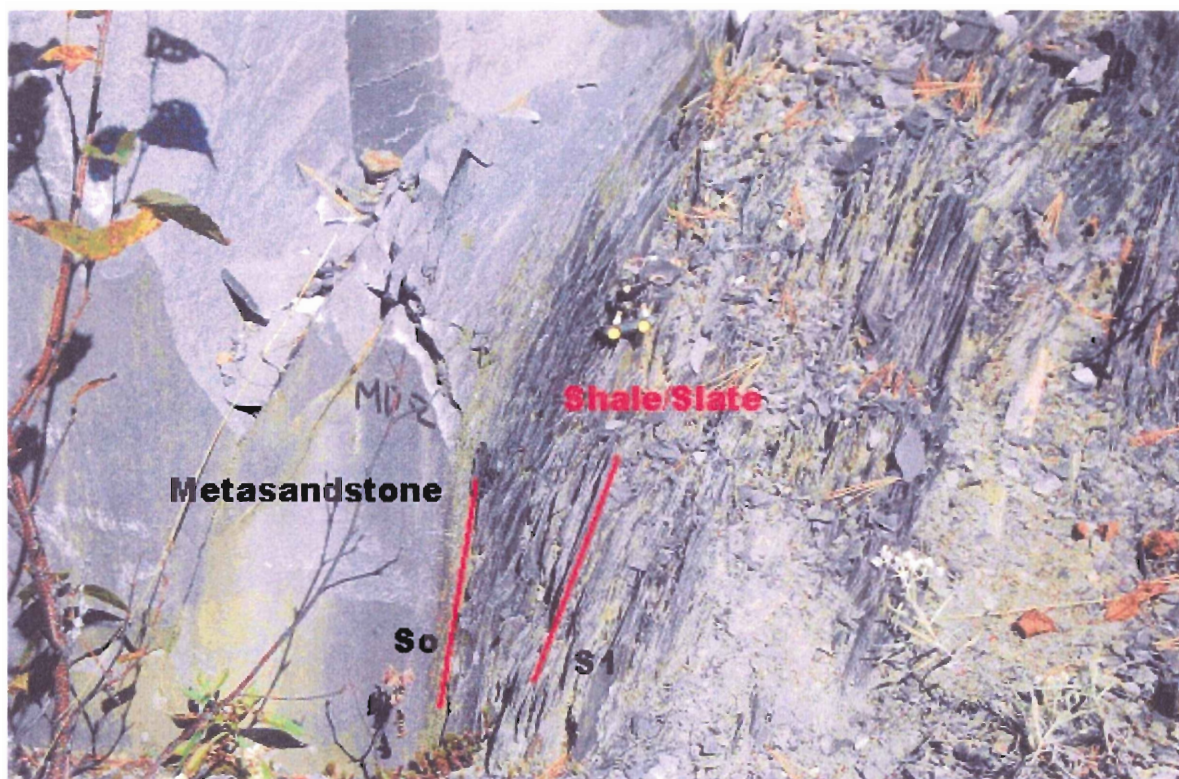
Figure 2.6: Station MD-2, Montague Drive, outside the gold district, on south limb of the Montague district fold. Same lithologies observed as inside the district; however no oikocrysts present. Bedding (S_0) and primary slaty cleavage (S_1) are trending and dipping in the same direction as within the district.

2.2.3 Other sample locations

Other samples were collected by Rick Horne (NSDNR), from the Mooseland and

Caribou districts prior to this thesis work. Samples at Mooseland were taken from loose

material and from diamond drill core ML-03-86, currently being analyzed by Bryan Rae for

his B.Sc. project. Samples from Caribou, which is in the Goldenville Formation 130 km

west of Halifax, near the South Mountain Batholith, were taken only from loose material

from the rock piles at the mine sites. Samples from North Brookfield were collected by

Chris White (NSDNR) from an outcrop near the hinge of the fold of the district,. These

samples were examined in order to compare them to the samples taken at Oldham and

Montague, in order to resolve any mineralogical or structural differences in the oikocrysts

between districts.

2.3 Fold Geometry Relationships

In the Meguma Group gold deposits, structural geometry plays an important role in

gold mineralization and oikocryst development. The particular fold geometry correlates

with the observed orientation of the oikocrysts. This suggests that the orientation of

oikocrysts are related to fold-related strain in the districts, further implying that oikocrysts

are pre- to syn- folding and that their elongation and distribution was affected by folding.

Figure 2.7 illustrates the basic terminology and principles used in the following discussion.

2.3.1 Oikocryst lineation and folding

The association of folds with a lineation defined by elongated features, like

oikocrysts, can offer insight into the conditions under which the oikocrysts and other strain-

related features formed. Typically, the orientation of the lineation, including oikocrysts, is

related to geometry of the fold hinges. Oikocrysts occur in the cleavage plane and their

long axes are perpendicular to the fold axis, which is parallel to the bedding-cleavage

intersection lineation (Fig. 2.8, 2.9). This perpendicular relationship is the same throughout

the all the deposits. As for most lineations that are perpendicular to the fold hinge, they

seem to be most strongly developed on the limbs and show little stretching in the hinge

zones, appearing rounder. Figure 2.10 (Twiss and Moores, 1992) shows lines on the

surface of a multilayer undergoing flexural-slip folding, which is at least one of the

deformation mechanisms that affected the gold districts in the Meguma Group (Horne and

Culshaw, 2001). The lines represent the long axes of oikocrysts at various locations along

the fold.

2.3.2 Gold district fold geometry

At the Oldham deposit, the fold is a doubly plunging anticline (Faribault, 1898).

Further analysis by Keppie (1976) interpreted the Oldham anticline to have a 45° conical

geometry in the NE and a 20° conical geometry in the SW. These conical terminations

represent the fold terminations (Keppie, 1985). The trend of the oikocryst lineation is

perpendicular to the fold hinge; therefore it varies throughout the district because of the

plunging nature of the dome. This relationship is identical at all of the districts. Horne et al.

(2003) demonstrated this relationship in stereoplots with data from the Mooseland Gold

district (Fig 2.11). Since the hinge is gently plunging, the plunge of the oikocryst lineation

is steep. This is consistent with the observations made in the field at all locations. At OLD-

6 near the plunging end of the Oldham dome, the plunge was 52° compared with stations

near the limbs where plunge were 75-85°.

At the Montague deposit, the anticline is a long, narrow, elliptical, doubly-plunging

anticline with the axis trending N78E with variable plunge (Malcolm, 1929). Near the fold

hinge the bedding dips shallowly to the north and south and the dip gradually increases
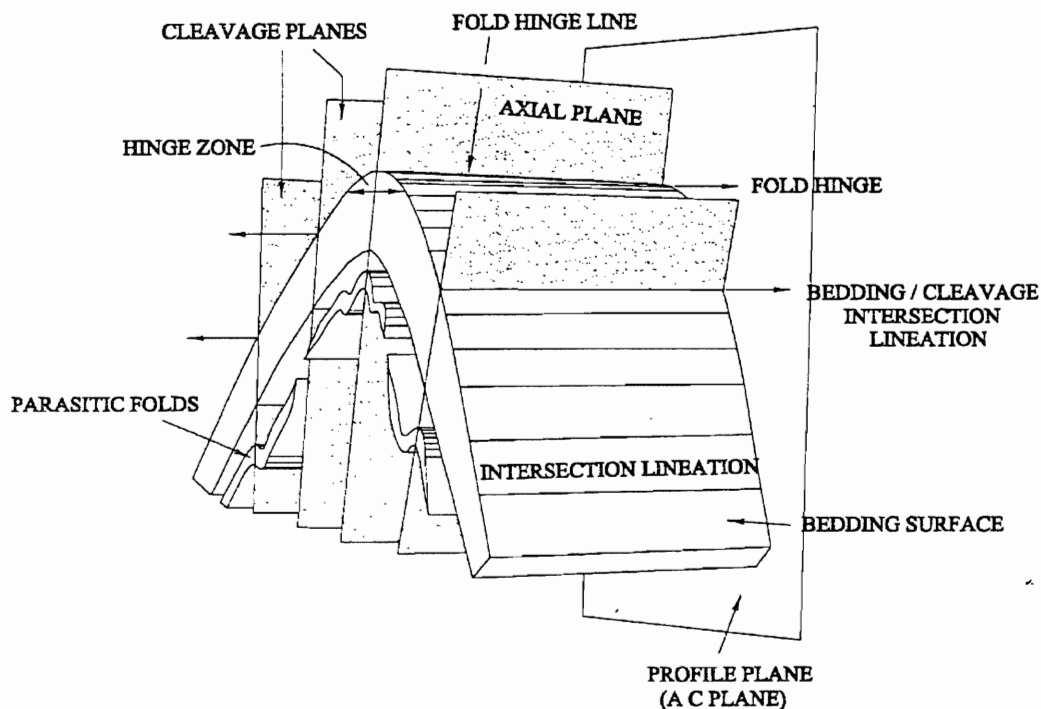
Fold hinge	A line connecting the points of maximum curvature of the fold
Fold hinge line	The line in the folded surface along which the curvature is a maximum
Hinge zone	The curved section of fold between planar limbs
Bedding cleavage intersection lineation	The line defined by the intersection of cleavage and bedding. The bedding-cleavage intersection is parallel to the fold hinge where cleavage is axial planar to the fold
Axial plane	A plane which bisects the limbs of the fold
Principal axis	The principal axes of the fold are, by convention: a axis is normal to the axial plane, the b axis parallels the fold hinge and the c axis is perpendicular to the hinge and contained within the axial plane.
Intersection lineation	The intersection of two planar elements
Cleavage plane	A surface of a specific orientation along which a rock has a tendency to break
Bedding plane	A well-defined divisional surface that separates two stratigraphically or lithologically different beds
Profile plane	A plane which is perpendicular to the fold hinge and contains the a and c fold axes

Figure 2.7: A schematic diagram showing the structural features of a fold with a table defining the terminology. (after Boulter, 1989)
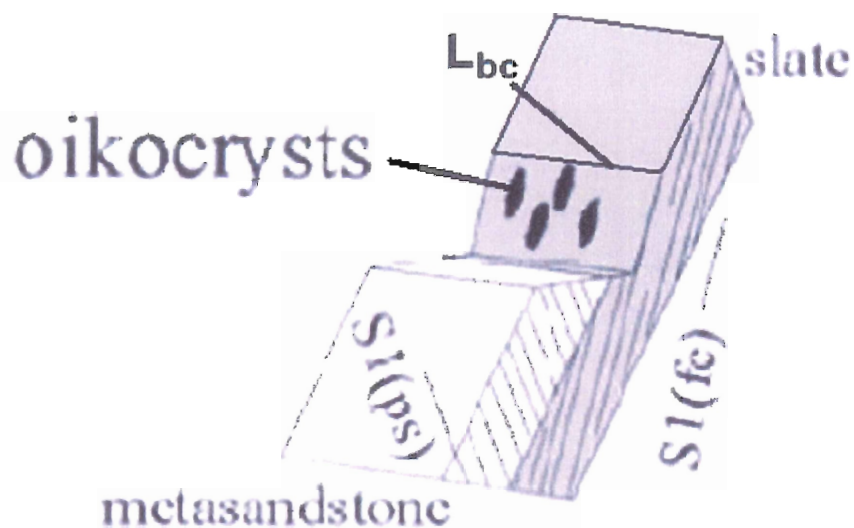
Figure 2.8: A schematic diagram showing outcrop-scale structural elements related to Meguma gold district anticlines; L_{bc} =bedding-cleavage intersection; $S_{1(fc)}$ = fine continuous slaty cleavage; $S_{1(ps)}$ = spaced pressure solution cleavage in metasandstone; which results from solution and removal of material during folding (after Horne et al. 2003).
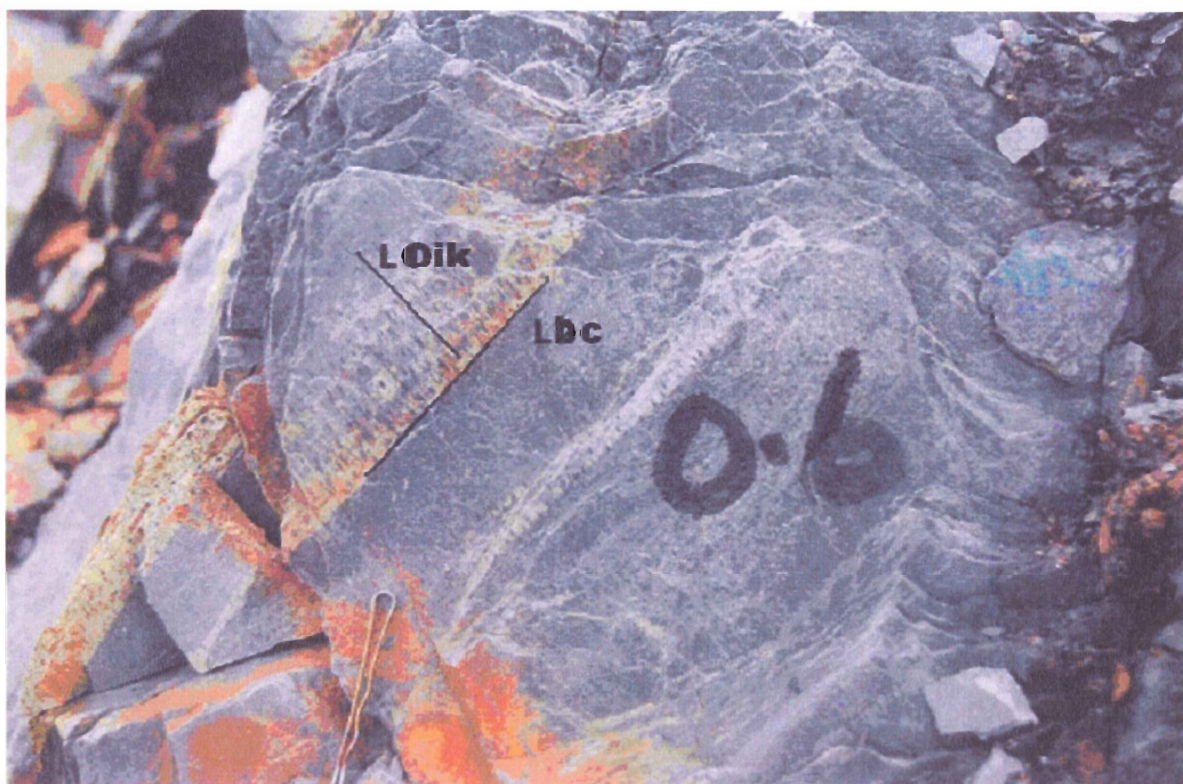
Figure 2.9: Station OLD-6 outcrop showing oikocryst lineation L_{oik} (281, 52) concentrated in lighter bed, extended perpendicular to bedding-cleavage intersection lineation L_{bc} (081/40) defined by boundary between the light and dark beds (Bedding 326/58) (bobby pin for scale).
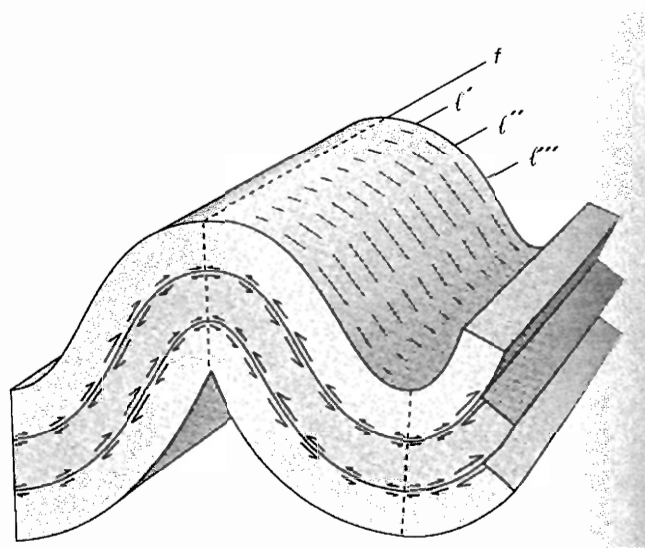
Figure 2.10: Flexural-slip folding in a multilayered sequence, which is one of the fold mechanisms affecting the gold deposits (Horne and Culshaw, 2001). An originally planar sequence of rock is folded; displacement on the layer surfaces is represented by the arrows. The shear sense reverses across the hinge line. The lines on the top surface represent the orientation of long axes of lineations like oikocrysts that record relative amounts of slip and strain (after Twiss and Moores, 1992).

(a)   (b)

. pole to bedding   , pole to cleavage (slate)

                                   + pole to cleavage (metasandstone)

                                   • oikocryst lineation

                                   ○ fold hinge
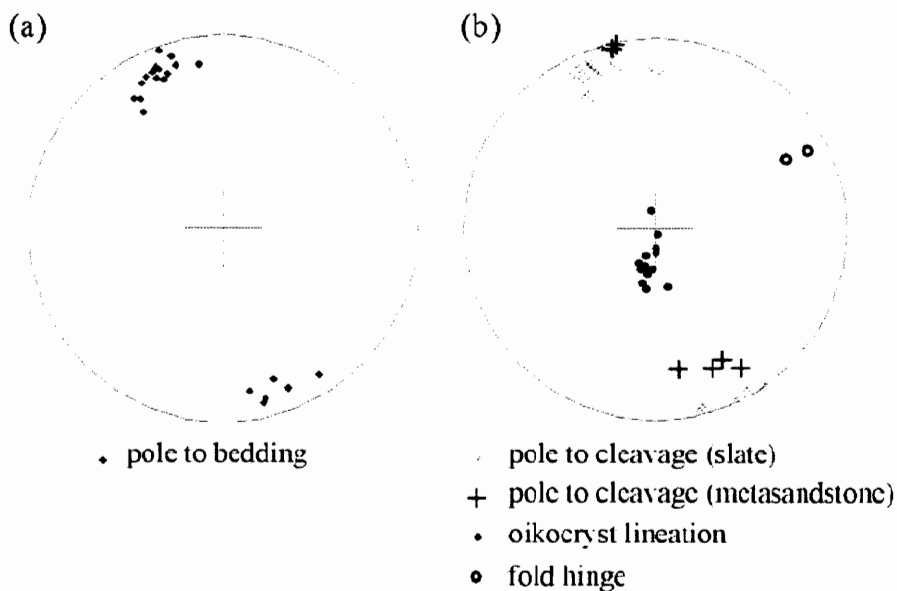
Figure 2.11: Lower hemisphere equal area stereoplots of structural data from the Mooseland Gold District. Both (a) and (b) present surface and underground data for the anticline (after Horne et al., 2003).

until it is vertical at approximately 1 km south and 7 km north of the fold hinge.

Therefore the axial plane dips 80° to the north. This was observed in the field, as the main

leads at Oldham and Montague strike parallel to the strata and dip shallowly to the south

(Malcolm, 1929). The Caribou and North Brookfield districts are also defined by

anticlines that trend northeast and have similar dome structures (Sangster and Smith,

2006).

At Mooseland, the fold geometry takes the form of steep, tight (inter-limb angle

of ~35°) NE-SW trending chevron folds with a well developed slaty cleavage that dips

steeply at a small angle to bedding (Horne et al., 2003). It was thought that the

Mooseland anticline was also a dome structure (Faribault, 1899a); however the bedding-

cleavage intersection lineations and fold hinges plunge consistently to the east. Saddle

reefs are present in the thickened hinge zones of the chevron folds (Horne et al., 2003).

In general all of the Meguma Group districts have similar fold geometry and

orientation, with related smaller-scale structures. Most of the gold deposits occur in the

northeast-trending anticlines with conical terminations (Keppie et al., 2002), or in tighter

chevron folds. In both cases bedding-parallel quartz veins are the dominant gold-hosting

veins.

Chapter 3

PETROGRAPHY

3.1 Introduction

Oikocrysts exist in both the metasandstone and metasiltstone units of the Goldenville Formation. Samples were taken from units both inside and outside the gold districts visited for this study. This chapter summarizes the general mineralogy and textures of these two units and of the oikocrysts. After petrographic and microprobe analysis the oikocrysts were classified into four types based on the mineralogy and texture of their aggregate interiors and rims.

3.2 Metasandstone and Metasiltstone Assemblages and Textures

The Goldenville Formation is dominated by metasandstone beds 0.5-1 m thick, with a variable amount of interbedded metasiltstone and slate in different areas. In most of the gold districts studied, the gold-bearing veins were concentrated in <1m thick olive green metasiltstone, with <1m thick dark black slate observed only at the Oldham district (Horne, 1996). The metasiltstone is dominated by fine-grained subidio- to xenoblastic quartz, feldspar, and fine-grained to microcrystalline, idio- to xenoblastic chlorite and muscovite, with minor accessory minerals including fine- to coarse-grained sulphides, oxides and carbonate (Fig. 3.1). A bedding-parallel planar foliation (S_o) is defined by the compositional layering, and the alignment of microcrystalline white mica and chlorite defines a foliation (S_1) which is more easily observed in the slate (Fig. 3.2). The oikocrysts define a lineation, which is within S_1. There is also a large amount of medium to coarse-grained subidioblastic detrital quartz and feldspar in the metasiltstone that is not

prominent in the slate. There are commonly very fine-grained inclusions of Fe-sulphides and Fe-oxides within these quartz and feldspar detrital grains.

The slate is generally darker than the metasiltstone, and has a strong cleavage in most outcrops. It consists of a microcrystalline matrix of aligned mica and chlorite with very fine-grained granoblastic quartz and feldspar. The amount of chlorite differs from sample to sample. Tabular idio- to subidioblastic muscovite is more prominent in the slate than in the metasiltstone and forms medium-grained porphyroblasts at an angle to S_1 and L_{oik} (Fig. 3.3), contributing to a late schistosity (S_2). This is observed only at Mooseland and Montague, commonly with chlorite strain shadows with radial extinction (Fig. 3.4).

Porphyroblasts of sulphides, oxides, and carbonate were observed in many samples from both lithologies. Some of them share similar properties. In some samples they have strain shadows of coarse-grained quartz or coarse-grained chlorite. In many cases the sulphides are oxidized, shown by embayed grain boundaries, and the carbonate is recrystallized. Finer oxide grains present throughout matrix generally are idioblastic and help define the late schistosity S_2 (Fig. 3.5). The coarse-grained sulphides, typically arsenopyrite in Mooseland district samples, are closely related to oikocrysts in some samples where single coarse grains of arsenopyrite form the cores of the oikocrysts. This relationship will be discussed further in Chapter 4.

Fine- to medium-grained subidio- to xenoblastic biotite is a dominant porphyroblast that also defines a late schistosity (S_2) in some slides, especially in the metasiltstone samples at Montague and Mooseland, and is closely associated with idio- to xenoblastic chlorite. Chlorite is replacing biotite in these slides and in the rim of some
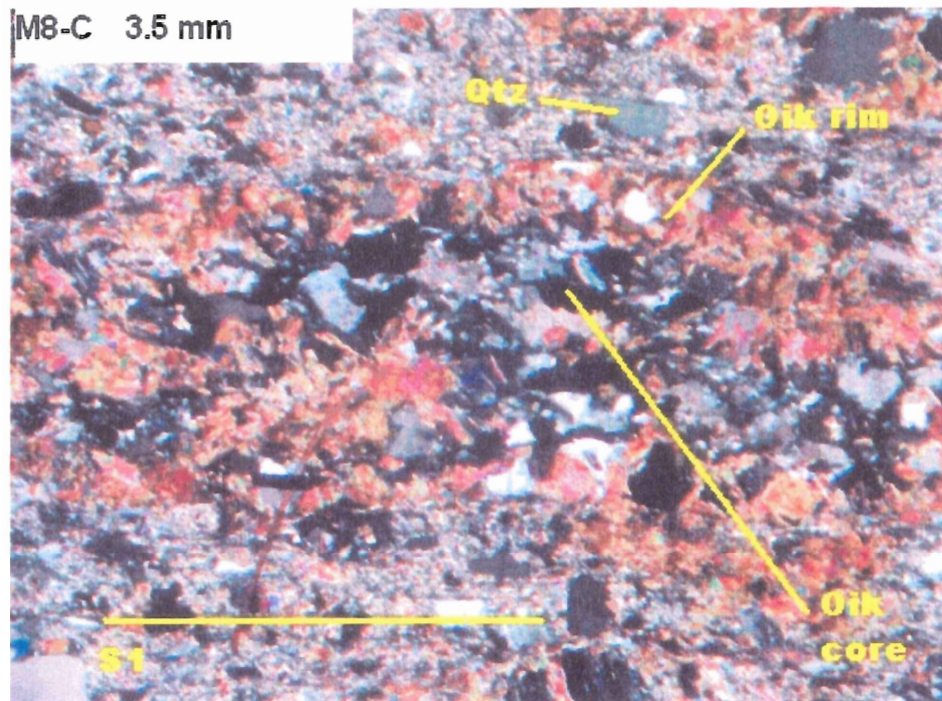
Figure 3.1: Sample M8-C: Stacked oikocrysts in Montague metasiltstone layer with coarse detrital quartz and feldspar (XN).
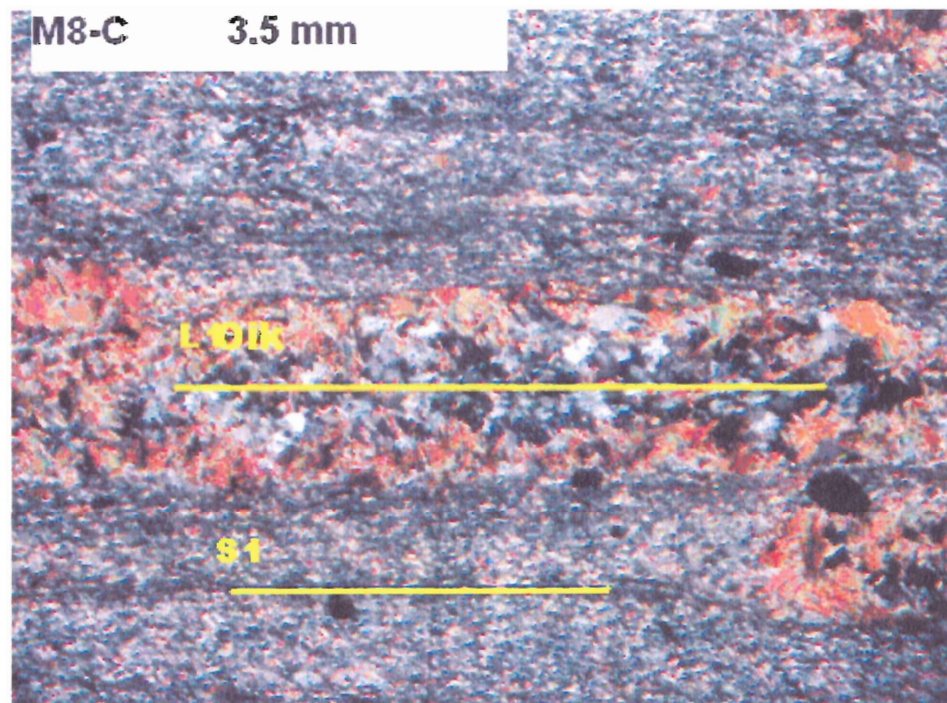
Figure 3.2: Sample M8-C: An oikocryst from Montague in a compositionally banded slate (XN).
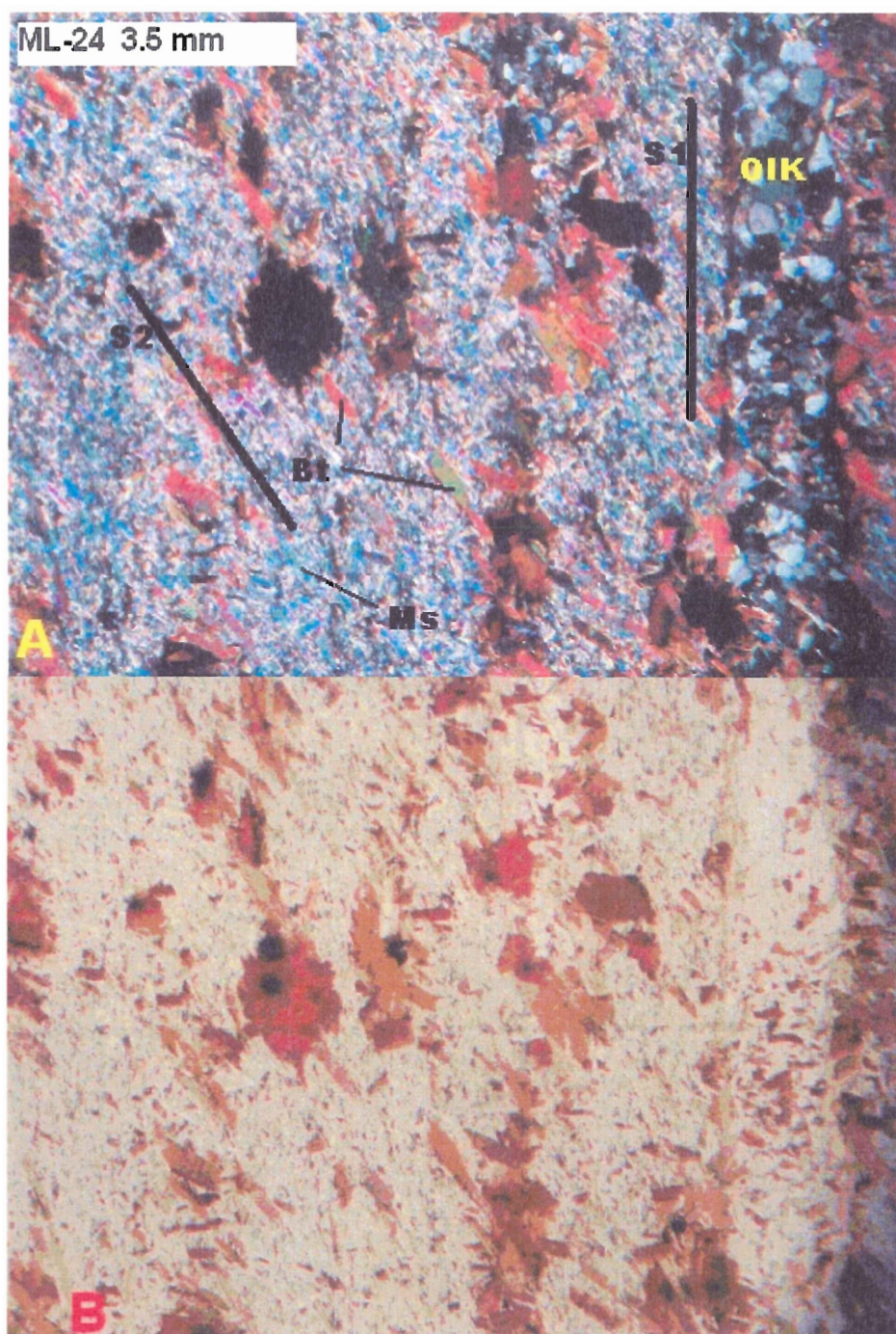
Figure 3.3: Sample ML-24 from Montague: A weak schistosity (S2) defined by muscovite, and biotite, that is at an angle to the main foliation (S1) and to oikocrysts. A) XN; B) PPL.
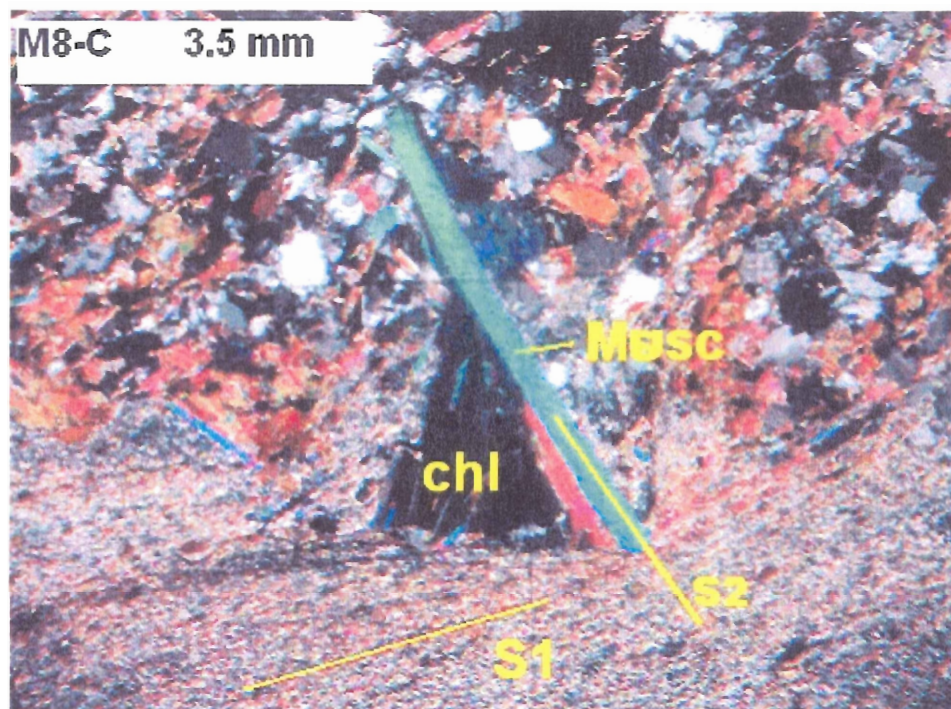
Figure 3.4: Sample M8-C from Montague: Muscovite with a chlorite strain shadow between a slate and metasiltstone layer. (XN).
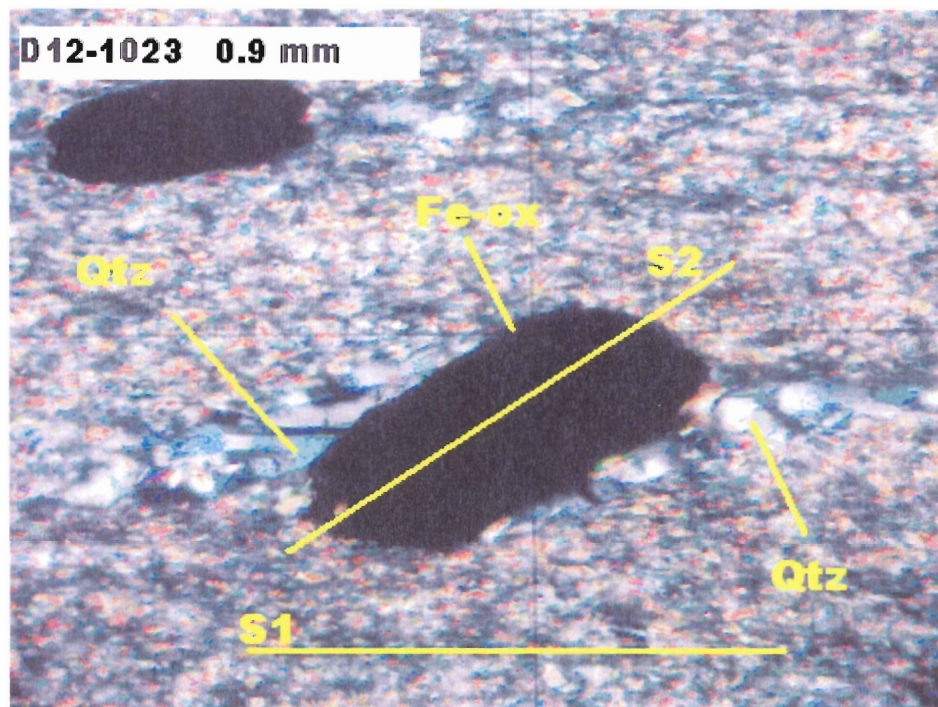
Figure 3.5: Sample D12-1023 from Mooseland drill core: Rotated Fe-oxide defining S_2 inclined at an angle to the main foliation (S_1) with strain shadows of coarse grained quartz (XN).

oikocrysts (Fig 3.6). Some samples are biotite-free, with chlorite more dominant in the matrix, where it defines the matrix foliation along with muscovite (S_1). In other cases, biotite is on its own with no chlorite replacing it. This chlorite-biotite relationship seems to be reflected in the oikocryst structure, mineralogy, and texture, as discussed in the following section. Muscovite porphyroblasts are commonly intergrown with the biotite and chlorite.

3.3 General Features and Classification of Oikocrysts

Oikocrysts are described here in terms of a two-component structure; their interiors and their rims. Some have rounded edges at their extremities and others come to a point. The aspect ratio ranges from 4:1 to 12:1, and is related to the amount of strain experienced by the rock in proximity to the fold hinge. Localized shearing gives sigmoidal asymmetric shapes to the oikocrysts and to other porphyroblasts within the same sample (Fig. 3.7). Their internal mineralogy varies but is generally dominated by fine- to coarse-grained granoblastic quartz, medium-grained subidio- to xenoblastic chlorite, and also a minor amount of medium- to coarse-grained subidio- to xenoblastic carbonate. The rims can vary in thickness and mineralogy. They are dominated by chlorite (X_{Mg} = 0.41-0.47) intergrown with biotite (X_{Mg} = 0.38-0.92) with chlorite replacing biotite to different degrees depending on the sample (for full compositional data see Appendix A). There is no sharp contact between the rim and the interior; instead elongated chlorite and biotite grains in the rims extend into the interior giving the contact a jagged and in some cases gradational look. Some muscovite and opaque minerals of similar size and concentration to those seen in the matrix are intergrown or lie within the
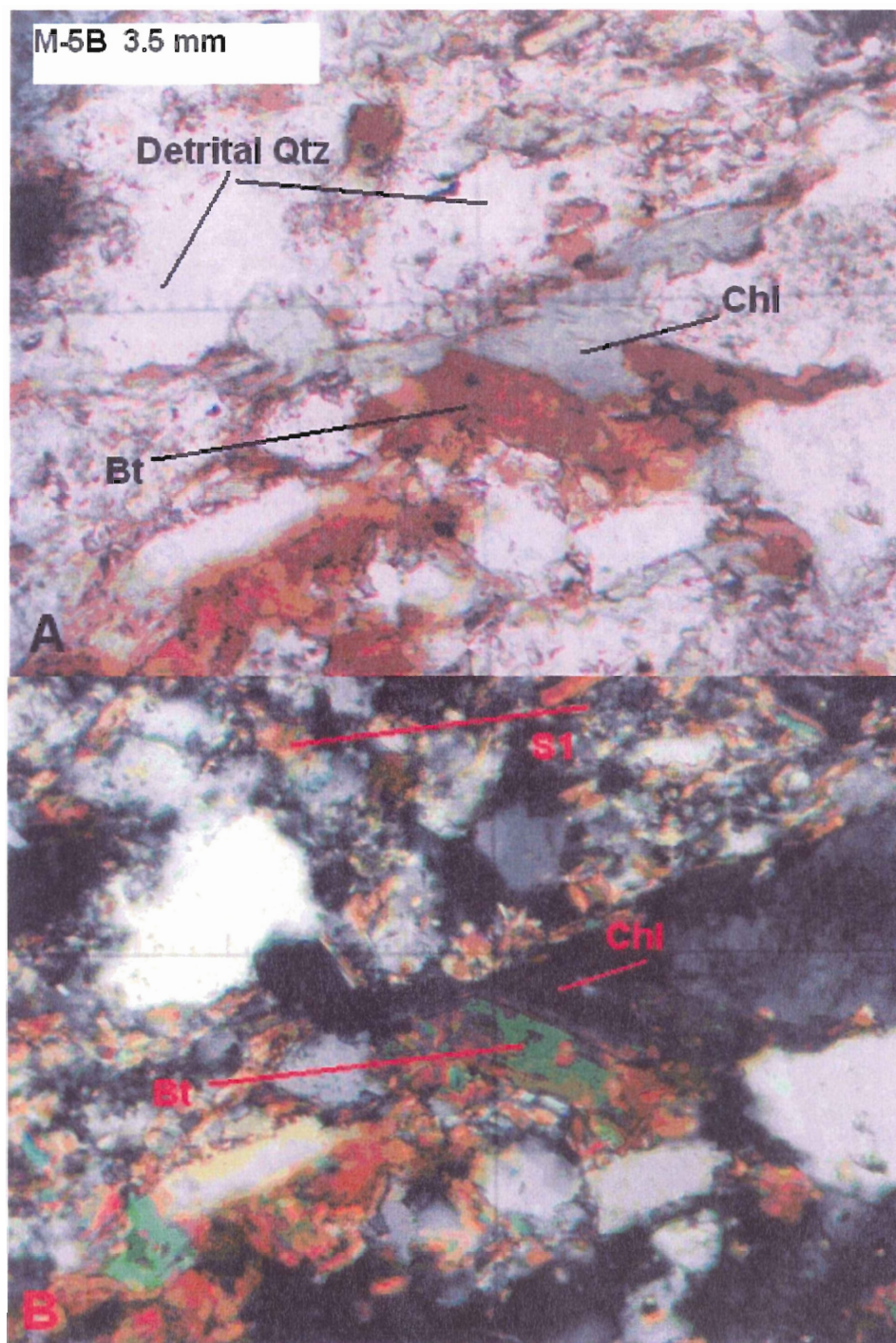
Figure 3.6: Sample M5-B from Montague: Biotite is being replaced by chlorite in a
detrital quartz-dominated metasiltstone sample. S_2 is not visible in this sample. A)
PPL; B) XN.
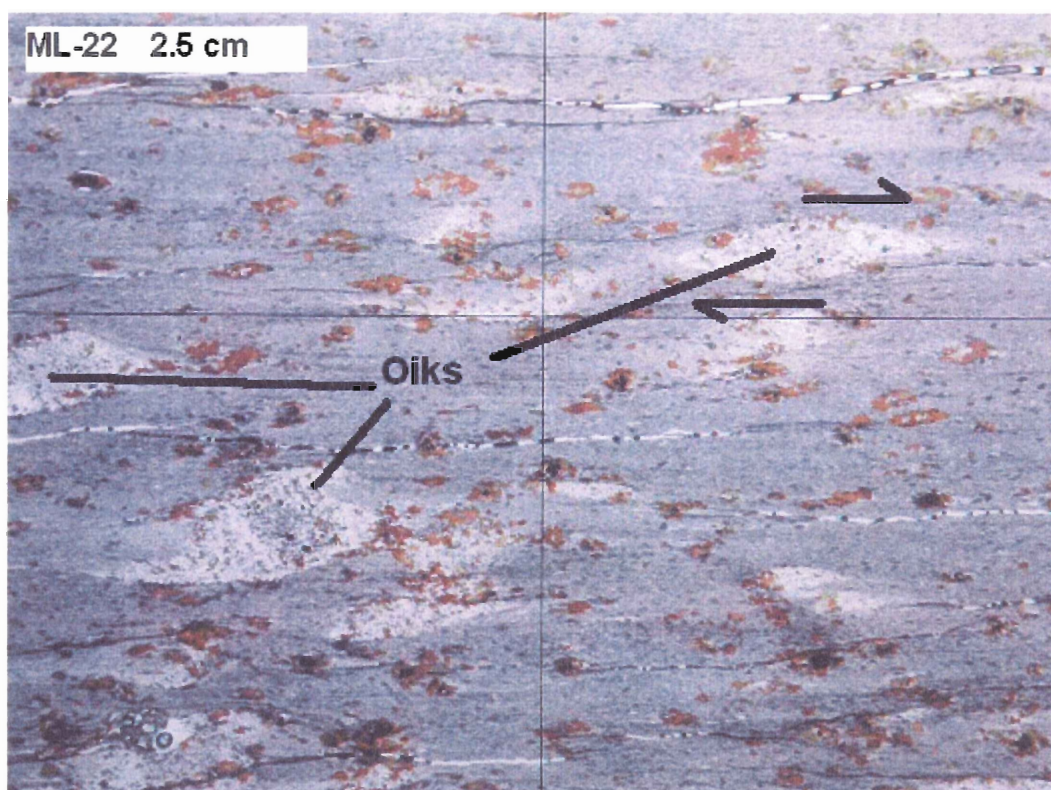
Figure 3.7: Loose sample ML-22 from Mooseland: Oikocrysts have a sigmoidal asymmetric shape in PPL suggesting dextral shear strain. No known relation to particular structural locations. S_1 and L_1 are oriented out of the page.

oikocryst completely. Minor fine- to medium-grained carbonate is also present in the rims of some oikocrysts.

One finding of this study is that the oikocrysts vary in structure between and within gold districts, depending on lithology. An attempt was made to classify the different types of oikocrysts after microprobe and microscope analysis of many different samples. Four main types are described below and summarized in Table 3.1.

3.3.1 Type I – Biotite-Chlorite Clusters - BCC

Biotite-chlorite clusters are apparently confined the medium- to coarse-grained metasiltstone. Biotite and chlorite seem to cluster between the detrital quartz and feldspar grains, giving the rock a "spotted" look under the microscope. They do not have a well-defined shape, but are strung out between the coarse grains. Unlike Types II, III, and IV, they do not form rims around an internal aggregate (Fig. 3.8). Medium to coarse-grained idioblastic muscovite is locally intergrown with the clusters.

3.3.2 Type II – Biotite-Chlorite Rimmed Oikocrysts - BCRO

Biotite-chlorite-rimmed oikocrysts are by far the most common type in the samples taken for this study, and are typical of oikocrysts in general. They are in both metasiltstone and slate in which biotite is present in the matrix. The thickness of the rims ranges from 50 μm to 500 μm, and the ratio of biotite to chlorite in the rims varies from oikocryst to oikocryst. In most samples, most biotite and chlorite grains in the rim align obliquely at a uniform angle to the matrix foliation (S_1); however in the strain shadows, they become parallel to S_1 (Fig. 3.9). The thickness of the rim is, however, not constant around the oikocrysts. The interior fabric of granoblastic quartz, carbonate and feldspar is

coarser than that of the slate matrix, yet very similar to that of associated metasiltstone layers.

3.3.3 Type III – Chlorite Rimmed Oikocrysts - CRO

These oikocrysts are rimmed only by chlorite, and chlorite is the dominant internal phase (Fig 3.10). They can be more difficult to distinguish from the matrix under the microscope because of their lack of a red/brown rim; they are "naked" oikocrysts. Their edges are defined by the finer-grained matrix fabric aligned with the edge of the oikocryst and deflected around its tapered edges. The chlorite grains that make up the rim are aligned similarly to the grains in the biotite-only rims, and seem to all extinguish at once when the slide is rotated. If coarse muscovite is present in the matrix, it is intergrown with the oikocryst. The amount of interior quartz varies, and has the typical coarse-grained, granoblastic texture.

3.3.4. Type IV – Biotite-Rimmed Oikocrysts - BRO

The biotite-rimmed oikocrysts do not have any chlorite replacing the rim material, and the interior of the oikocryst contains biotite and little to no chlorite (Fig. 3.11). This type is more common in the biotite-rich metasiltstones at Mooseland that have been affected by contact metamorphism. The rim can vary in thickness, and the biotite has a general preferred orientation perpendicular to the matrix foliation.

3.4 Sulphides within Oikocrysts

If the mineral assemblage of a sample contains sulphides, the sulphides always associate spatially with the oikocrysts. Many oikocryst samples have cores that are dominated by coarse-grained xenoblastic porphyroblasts of arsenopyrite, and
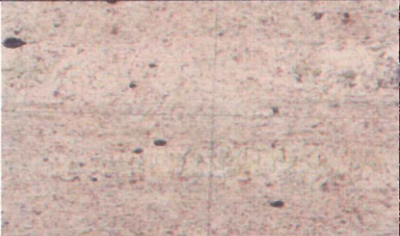
Oikocryst Type	Photo in PPL (field of view = 1.7mm)	Localities Observed	Rim Texture and Mineralogy	Core Texture and Mineralogy	Matrix Texture and Mineralogy
Type I **Biotite-Chlorite Clusters**		Montague Oldham	n/a	NO CORE; m.g. subidioblastic biotite-chlorite intergrowths minor muscovite	f.g.-m.g. metasiltstone foliated white mica, chl m.g. detrital quartz m.g. carb and albite idioblastic m.g bt & musc defining S_2 minor oxides & Fe-slph
Type II **Biotite-Chlorite Rimmed Oikocryst**		Montague Oldham Mooseland Caribou	subidioblastic biotite, chlorite, muscovite aligned with S_2 in some cases	m.g. granoblastic quartz and albite f.g.-m.g. muscovite, chlorite, biotite, minor sulphides	f.g-m.g. metasiltstone/slate foliated white mica, chl m.g. detrital quartz m.g. carb and albite idioblastic coarse bt & musc defining S_2 minor oxides & Fe-slph
Type III **Chlorite-Rimmed Oikocryst**		Oldham Caribou North Brookfield	f.g. subidioblastic chlorite minor muscovite aligned with S_2	m.g. granoblastic quartz m.g.carbonate and albite f.g.-m.g. chlorite and muscovite	f.g.-microcrystalline slate foliated white mica, chlorite and muscovite f.g. quartz, carbonate and albite minor oxides & Fe-slph
Type IV **Biotite-Rimmed Oikocryst**		Mooseland	m.g. subidioblastic biotite minor muscovite aligned with S_2	m.g. granoblastic quartz m.g. carbonate and albite f.g.-m.g. biotite muscovite minor sulphides	f.g.-m.g. metasiltstone/slate foliated white mica m.g. detrital quartz m.g. carb & albite idioblastic c.g. bt & musc defining S_2 minor oxides & Fe-slph

Table 3.1: Classification table of oikocryst types based on the mineralogy and textures of the rim and core, with a link to the locations and lithologies in which they were observed. (f.g.-fine-grained, m.g.-medium-grained, c.g.-coarse-grained)
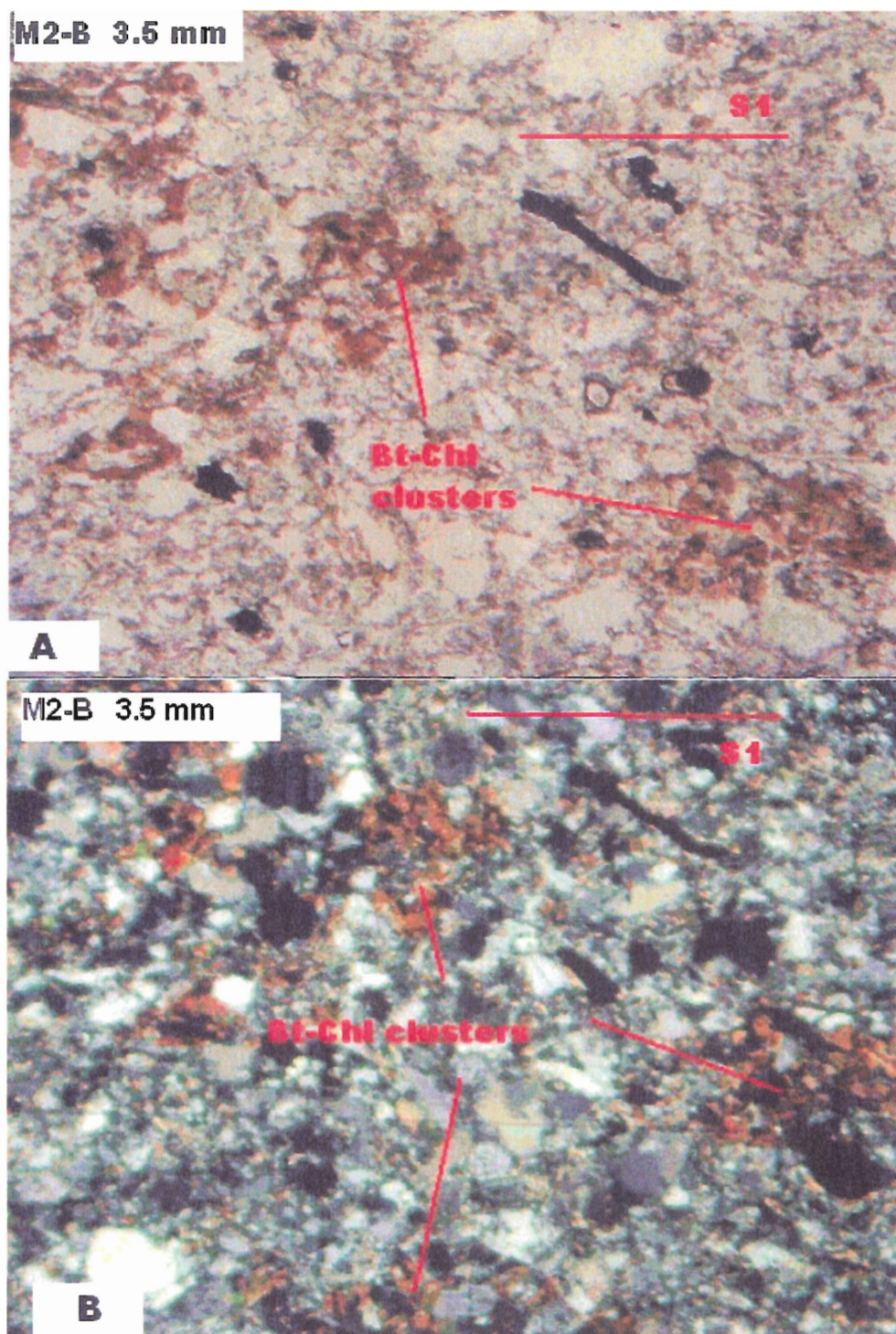
Figure 3.8: Sample M2-B from Montague: Type I – Biotite-chlorite clusters in metasiltstone layer. S_2 is not visible here. A) PPL; B) XN.
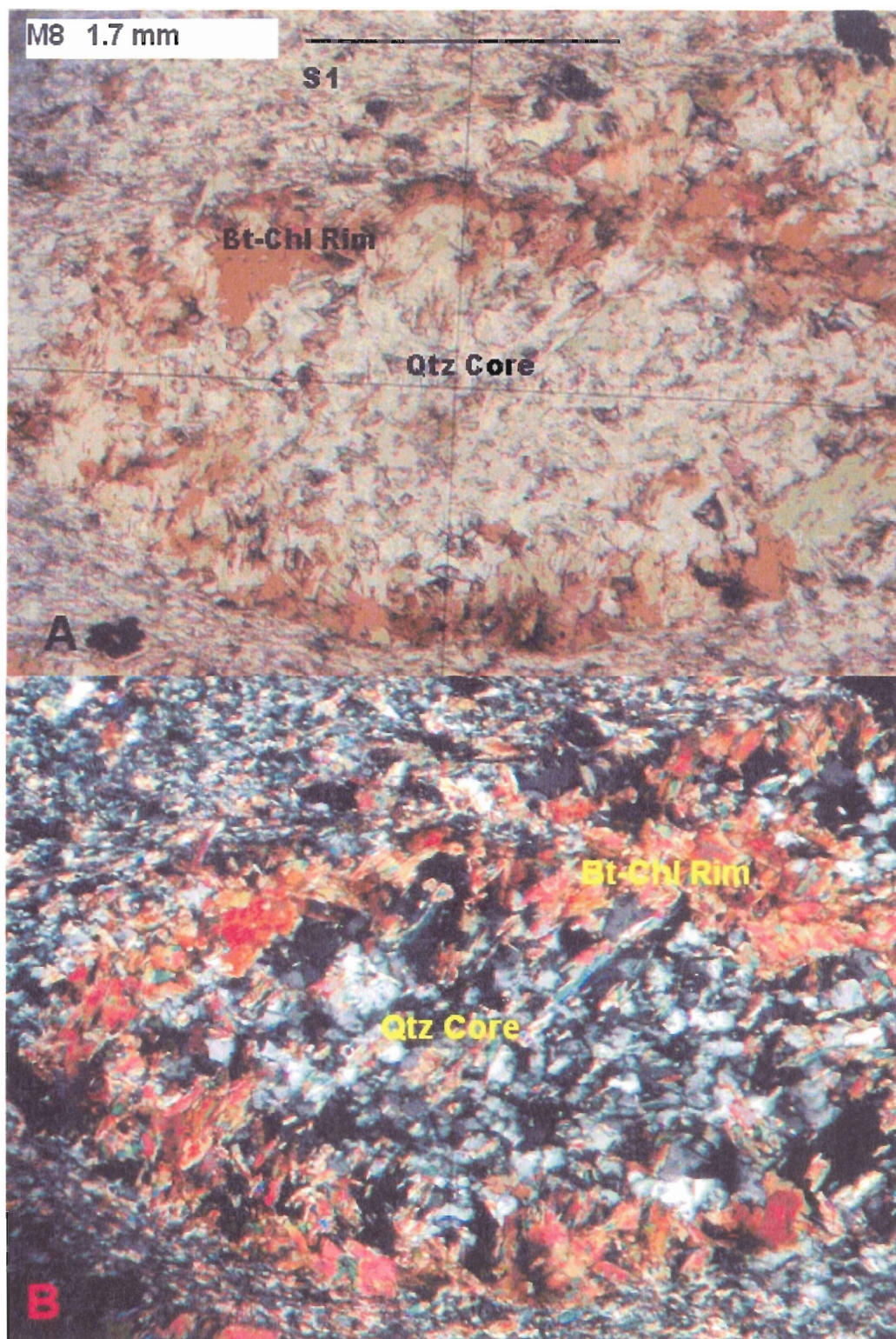
Figure 3.9: Sample M8: Type II – Biotite-chlorite rimmed oikocryst from Montague with a quartz-dominated core (See BSE image: M8_C_A3, Appendix B). A) PPL; B) XN.
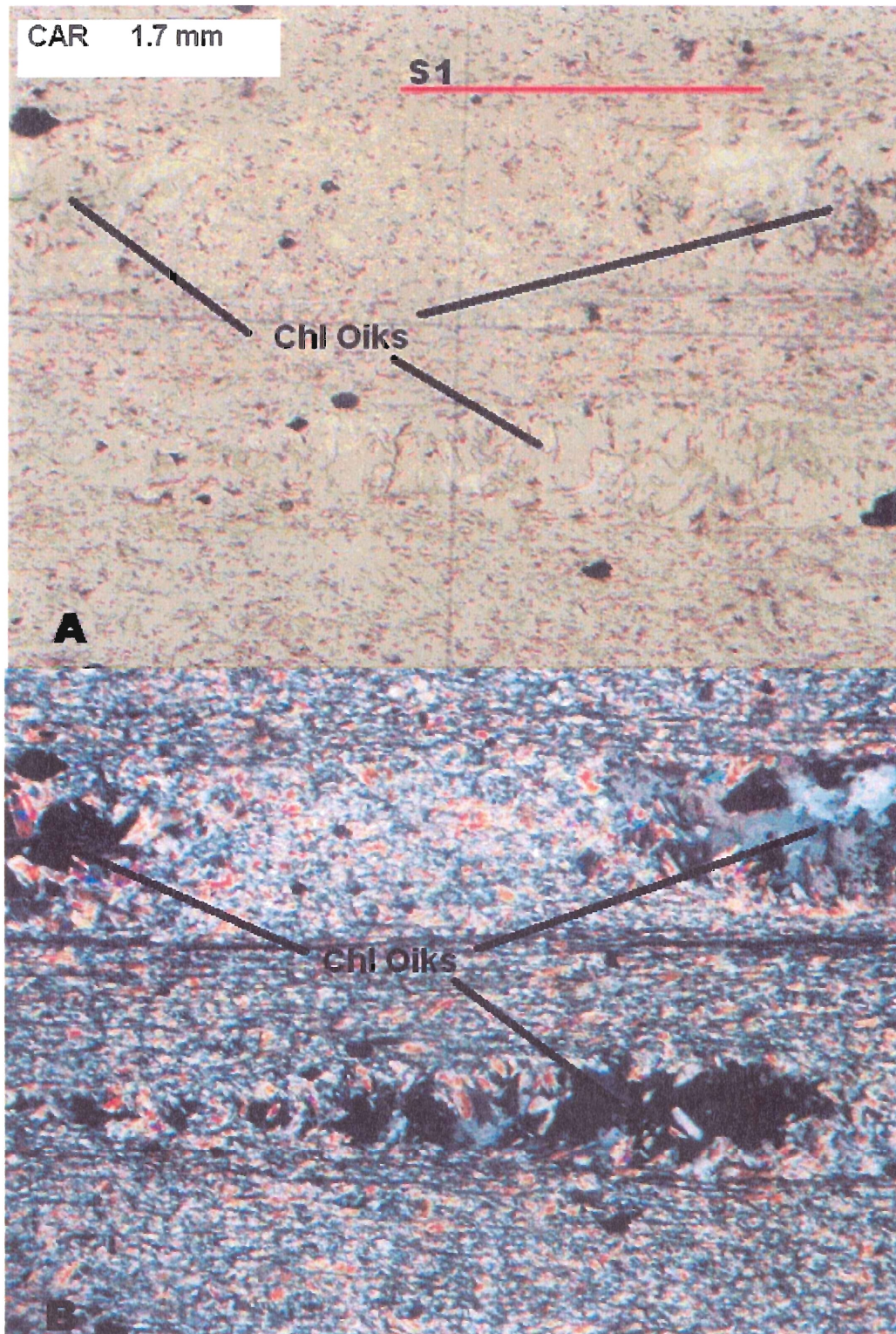
Figure 3.10: Sample CAR from Caribou: Type III – Chlorite-rimmed oikocryst in a slate layer. A) PPL; B) XN.

under reflected light, inclusions of fine-grained, embayed pyrrhotite, pyrite and chalcopyrite are revealed to be intergrown with them. These fine-grained sulphides are also observed on their own in the cores of oikocrysts and also in the matrix. In samples where arsenopyrite and other sulphides are intergrown, arsenopyrite seems to be growing while the other apparently less stable sulphides are dissolving. This is evident in the idioblastic texture arsenopyrite and the irregular grain boundaries of the other sulphides. Chapter 4 discusses this relationship in further detail.

3.5 Summary of Results

Variations on a basic oikocryst structure were found to be consistent throughout all the samples of oikocrysts used for this study. The cigar-shaped aggregates were shaped by regional strain and their petrography was determined by the sediment type and metamorphic grade. The structure and mineralogy of the rim varies with the lithology of matrix material, and the rims generally vary in thickness. There is a correlation between the oikocryst type and the district; for instance, if the district was affected by contact metamorphism (eg. Mooseland) and has porphyroblasts of biotite defining a late schistosity (S_2), the rim minerals generally have more biotite and are aligned with S_2. The alignment of the rim minerals is generally perpendicular or oblique to the matrix foliation (S_1) at all of the districts, and becomes parallel in the strain shadows. The oikocryst interiors typically resemble a coarser version of the matrix and are intergrown with the same porphyroblasts that are seen in the matrix.

Chapter 4

DISCUSSION

4.1 Introduction

The main objective of this thesis is to document the character of oikocrysts and to determine their relationship to other features in order to unravel their origin. Through petrographic and microprobe analysis a number of relationships were found that may prove to be a link to the genesis of oikocrysts. Three main hypotheses surfaced and further observation allowed for their documentation and assessment. The first possibility is that the oikocrysts could be altered cordierite porphyroblasts. The second possibility is that oikocrysts replaced arsenopyrite and/or other sulphides. Lastly, oikocrysts could be isolated microlithons of metasiltstone layers in the slate.

4.2 Relationship between Cordierite and Oikocrysts

Cordierite is characteristic of contact aureoles in the Meguma Group (Jamieson et al., 2005). It is present at North Brookfield gold district as well as in other locations like Point Pleasant Park (Fig 4.10) where pelites and siltstones of the Halifax and Goldenville Formation are intruded by granitic plutons. In the sample from North Brookfield, the cordierite is very similar in shape and size to the oikocrysts (Fig. 4.1). Even though there is a resemblance between the two features the oikocrysts have a distinct interior fabric made up of granoblastic quartz, feldspar and carbonate. This fabric seems to be a relict of a texture and internal foliation that was present before the last phase of deformation and hydrothermal vein emplacement. In contrast, poikiloblastic cordierite, even though it is
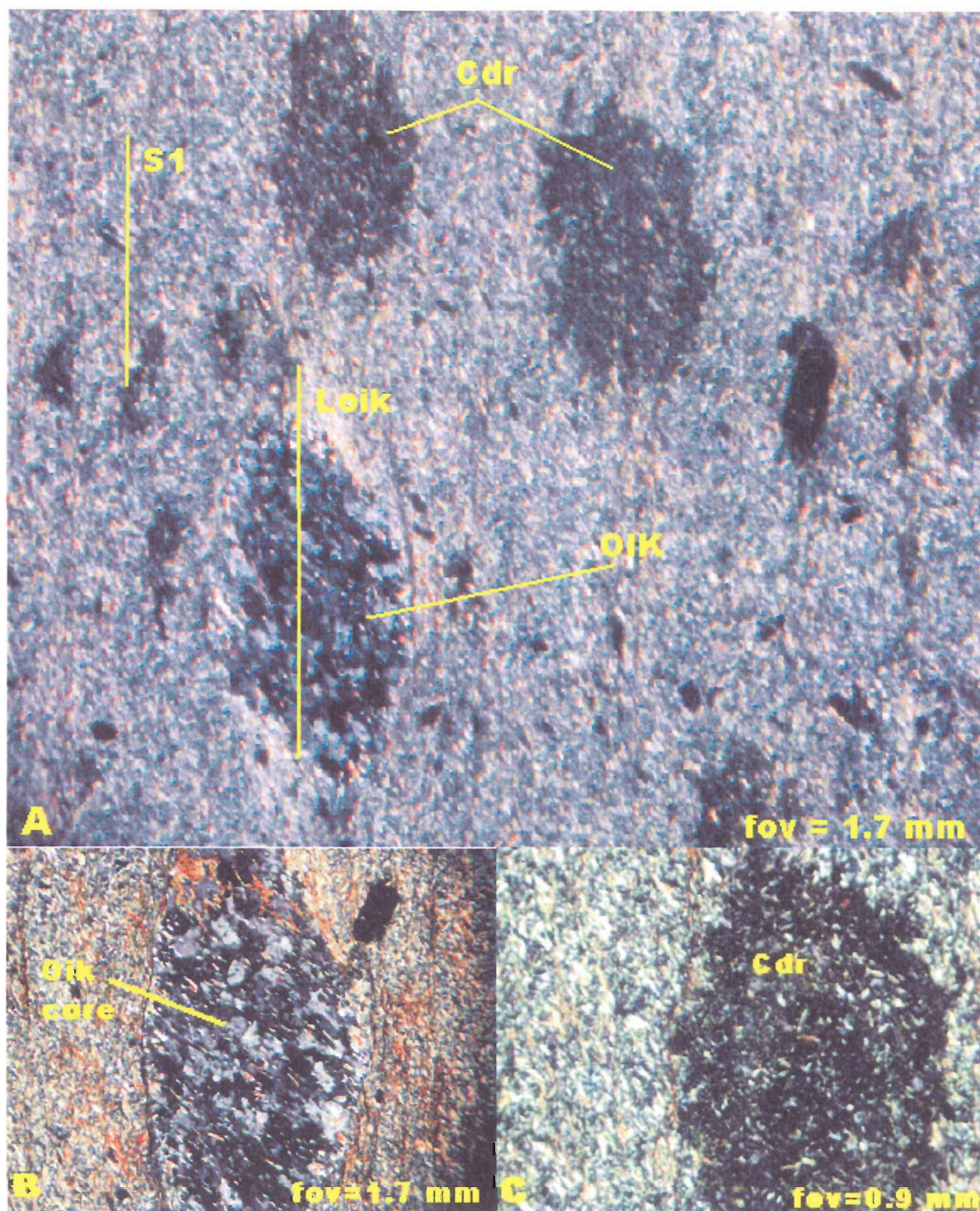
Figure 4.1: Sample from North Brookfield containing both cordierite and oikocrysts in A (XN), and a close-up of an oikocryst in B (XN), and cordierite porphyroblast in C (XN). Notice the relict foliation of minerals in the interior of the oikocrysts is at an angle to L_{oik}.

similar in aspect ratio, is characterized by fine-grained inclusions and pervasive alteration to sheet silicates. The two features are readily distinguished in thin section and it is concluded that oikocrysts in this sample and by implication, others are not altered cordierite porphyroblasts.

4.3 Relationship between Sulphides and Oikocrysts

One of the unique characteristics of oikocrysts is their close association with hydrothermal gold, arsenopyrite, pyrite, chalcopyrite, and pyrrhotite. Many of the samples collected for this thesis host a variety of these sulphide minerals that range from fine-grained matrix crystals to coarse-grained porphyroblasts. The coarse-grained sulphides are typically idioblastic, whereas the finer-grained sulphides are xenoblastic and have a spongy texture with embayed grain boundaries. Most of the grain boundaries have a rim of hematite, indicating oxidization.

Different gold districts display different interrelationships between sulphides and oikocrysts. For this study five sulphide-bearing samples with varying characteristics were chosen for observation under reflected light. Microprobe analysis was done on some of the main intergrown or isolated sulphides that were consistently associated with oikocrysts in some way.

Sample O3-A, a loose sample from an Oldham waste pile, has coarse porphyroblasts of arsenopyrite and a cm-scale quartz/carbonate vein, but no visible oikocrysts. In thin section under reflected light the arsenopyrite porphyroblasts have a coarse-grained, idioblastic texture and the fine-grained inclusions of chalcopyrite and pyrrhotite have embayed boundaries, suggesting that they wee overgrown by and/or

replaced by arsenopyrite. This suggests that arsenopyrite was growing and chalcopyrite and pyrrhotite dissolving in the metasiltstone matrix (Fig. 4.2, 4.3).

Mooseland samples are affected more by contact metamorphism than samples from other districts because of the proximity to the Musquodoboit Batholith. Numerous porphyroblasts of idioblastic arsenopyrite are visible in hand sample and in thin section. They are situated in the cores of Type II oikocrysts in a matrix that also has biotite porphyroblasts. Other minerals, predominantly pyrrhotite, pyrite, and chalcopyrite, form fine-grained, xenoblastic inclusions in the arsenopyrite porphyroblasts (Fig. 4.4). In the few oikocrysts that lack arsenopyrite porphyroblasts in these samples, small, embayed, remnant grains of pyrrhotite and chalcopyrite are found in the cores of the oikocrysts. Mooseland samples also feature coarse-grained ilmenite in the matrix. Some of these are elongated grains, parallel to S_1 and surrounded by a rim of chlorite or biotite (Fig. 4.5).

In contrast, samples from Caribou and Montague show no particular relationship between sulphides and oikocrysts. The Caribou sample has a few subidioblastic arsenopyrite porphyroblasts with quartz/chlorite strain shadows. There are also numerous subidio- to xenoblastic ilmenite and rutile grains in the matrix that have no special association with the Type III oikocrysts (Appendix B: sample CAR). The samples from Montague also lack large arsenopyrite porphyroblasts and do not contain many sulphides like the Oldham and Mooseland samples; however there are some randomly oriented ilmenite and rutile grains with no apparent association to oikocrysts.

A number of general observations can be made from comparing sulphide features with oikocrysts. Arsenopyrite grew where contact metamorphism affected the rocks, and
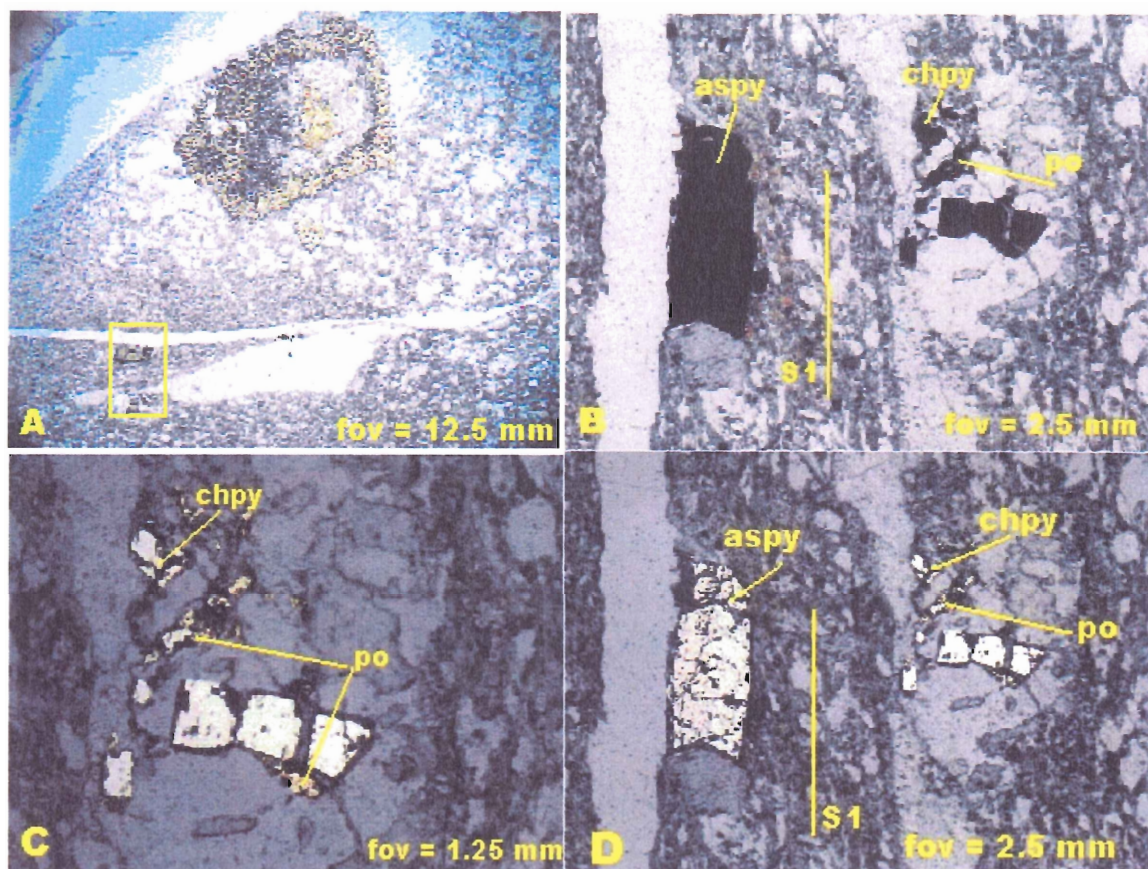
Figure 4.2: Sample O3-A from Oldham showing the difference between growing arsenopyrite and dissolving pyrrhotite and chalcopyrite in reflected light (A,C, D) and in PPL (B).
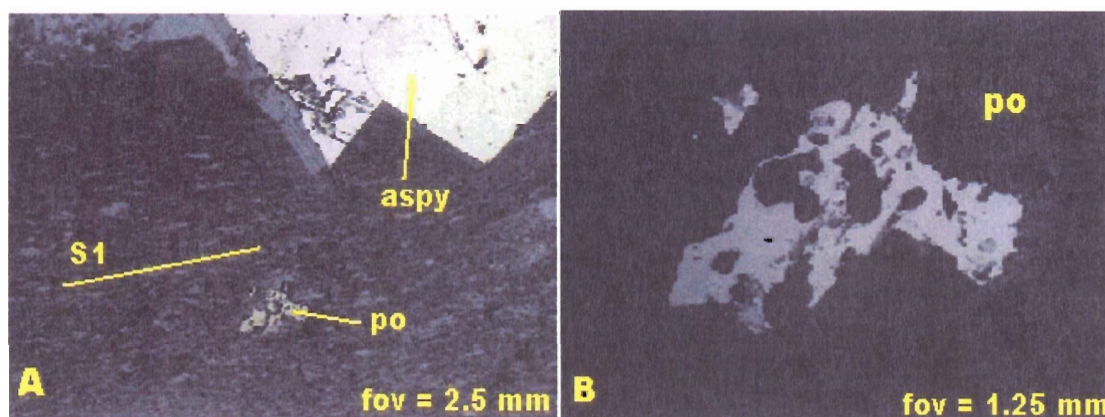
Figure 4.3: Sample O3-A from Oldham showing isolated xenoblastic, embayed pyrrhotite in the matrix. The irregular shape of pyrrhotite compared with arsenopyrite suggests that it was dissolving while arsenopyrite was growing (reflected light).
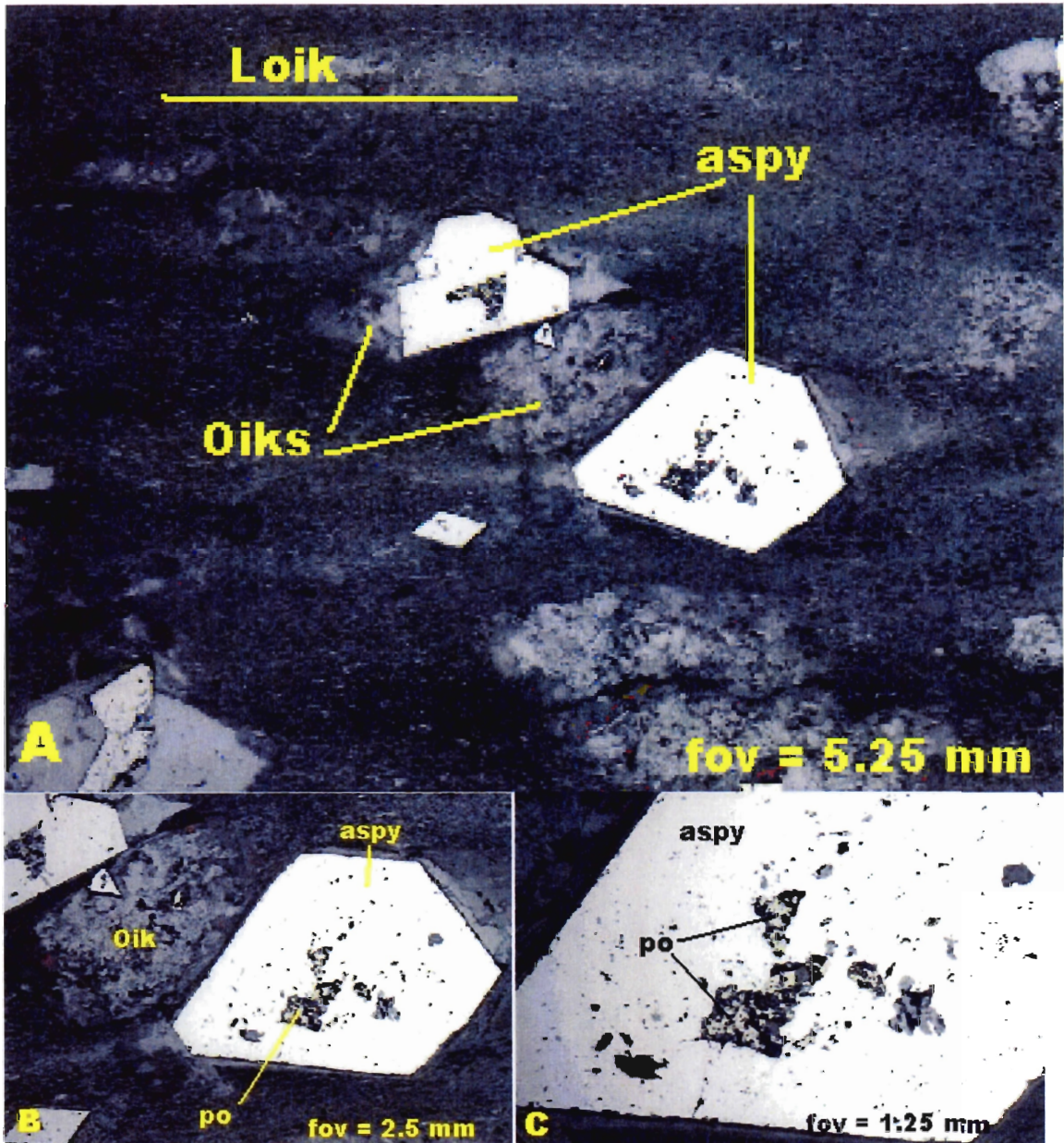
Figure 4.4: Sample ML-51B from Mooseland showing pyrrhotite inclusions inside an arsenopyrite porphyroblast, typical of many oikocrysts in the sample (reflected light).
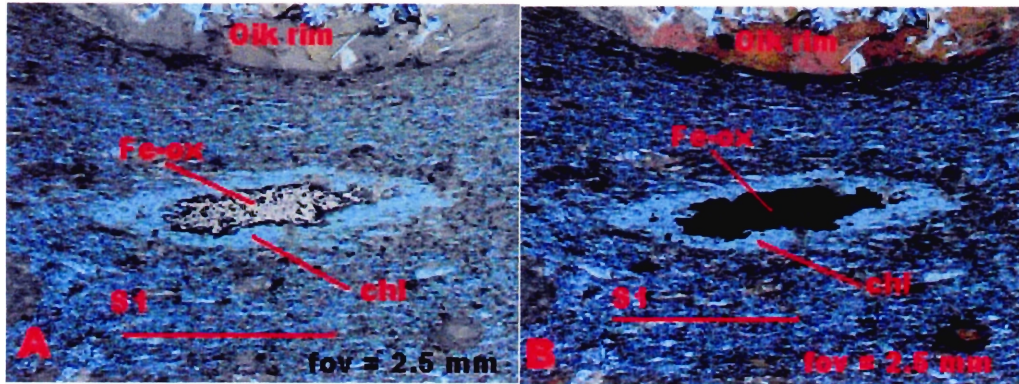
Figure 4.5: Sample ML-51B from Mooseland showing an elongated, coarse grained Fe-oxide grain with a rim of chlorite in (A) reflected light, and (B) PPL.

either makes up the interior of oikocrysts or is isolated in the matrix with a quartz/chlorite strain shadow. Xenoblastic grains of embayed relict pyrrhotite are closely related to the growing arsenopyrite, either nearby or as inclusions within the arsenopyrite. In conclusion, in some places there appears to be a correlation between sulphide and oikocrysts, but this is not observed in all districts.

4.4 Relationship between Microlithons and Oikocrysts

The deformation of the Meguma Group has led to the development of various foliations and lineations. One of these is a disjunctive or detached foliation which is common in low grade slates and metasiltstones (Twiss and Moores, 1992). It is characterized by cleavage domains that are marked by concentrations of strongly aligned platy minerals that separate tabular to lenticular domains of coarser grained material called microlithons (Fig 4.6). If platy minerals are present in the microlithons, they are less abundant or more randomly oriented than in the cleavage domains. Twiss and Moores (1992) describe four groups of disjunctive foliation based on the smoothness of

the cleavage domains – stylolitic, anastomosing, rough and smooth (Fig 4.6). These

groups can be subdivided based on the orientation and fabric of the microlithons; which
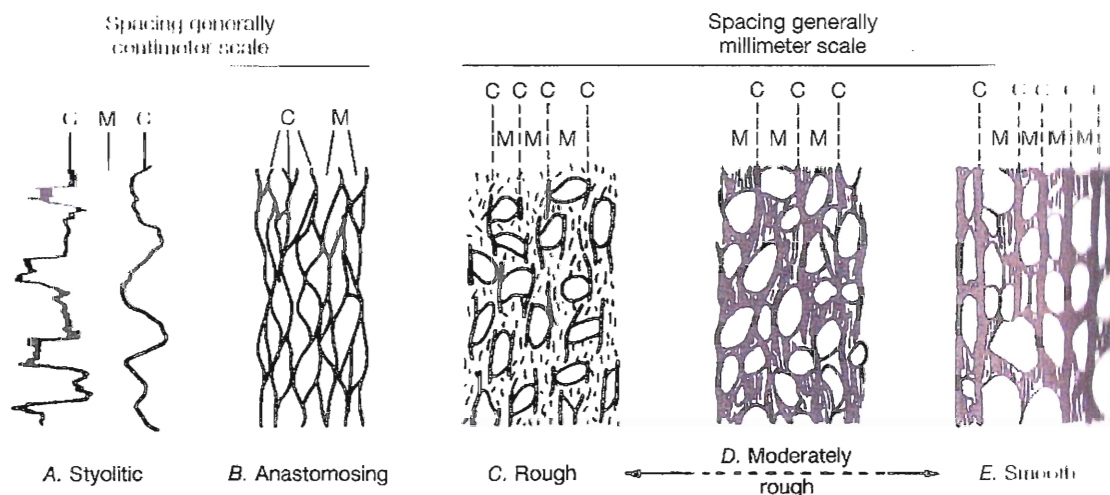
Figure 4.6: The various types of disjunctive foliation from centimeter to millimeter scale, where C defines the cleavage domains and M defines the microlithons. (Twiss and Moores, 1992, Fig 13.3)
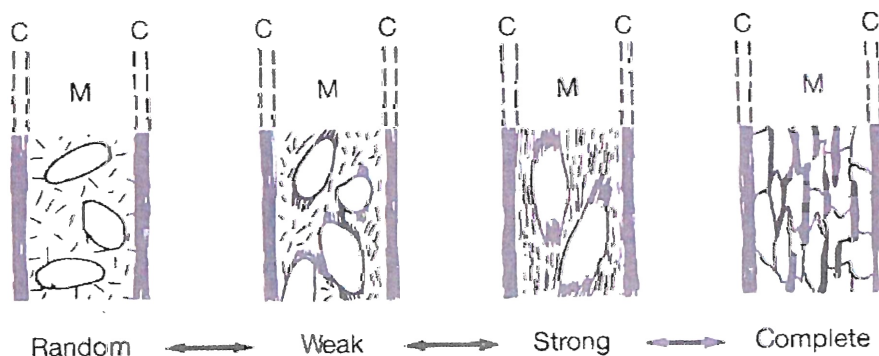
Figure 4.7: Further subdivisions of disjunctive foliations based on the fabric of the microlithons ranging from random to complete. C defines the cleavage domains and M defines the microlithon domains. The microlithon fabric progresses towards elongated mineral grains with preferred orientation, and strong alignment of the platy minerals in the matrix. (Twiss and Moores, 1992, Fig 13.4)

ranges from random to well oriented (Fig. 4.7). The Meguma Group oikocrysts have

many similar features to 'strong' microlithons in that they feature a distinct elongation of

isolated mineral aggregates, strong alignment of their long axes, and strong alignment of

the platy minerals in the matrix, and in some cases mica strain shadows. A 'rough'

disjunctive foliation is common in sand-sized mineral grains and a 'smooth' disjunctive foliation is characteristic of slates, therefore oikocrysts may represent 'moderately rough' disjunctive foliation, based on the lithology of the rocks.

In the thin sections that show slate and metasiltstone layers in contact, there is clearly a 'cusp and lobe' structure on the metasiltstone-slate contact (Fig. 4.8, 4.9) locally leading to isolation of siltstone in slate. This may be an early phase in the creation of oikocrysts, and may indicate that oikocrysts are microlithons of metasiltstone layers that have been subjected to high strain. The cusps have a rim mineralogy and texture similar to that of the oikocrysts, further suggesting a link to oikocrysts.

This is not the only location in the Meguma Group where a cusp and lobe structure is observed between coarse- and fine-grained lithologies. For example, they are also observed in Point Pleasant Park in Halifax Formation samples, which also contain cordierite (Fig 4.10). This verifies that the strain experienced by the Meguma Group lithologies has the potential to create disjunctive foliations and microlithons in locations other than antiformal gold districts.

4.5 Relationship of Oikocrysts to Gold Districts

It does not seem possible for either the microlithon hypothesis or sulphide hypothesis alone to explain both the formation of oikocrysts and their association with gold districts. It would be quite a coincidence if oikocrysts happened to occur where sulphides were accumulating because of the fold geometry of the districts. In order to rule out this coincidence more systematic and extensive outcrop mapping is required
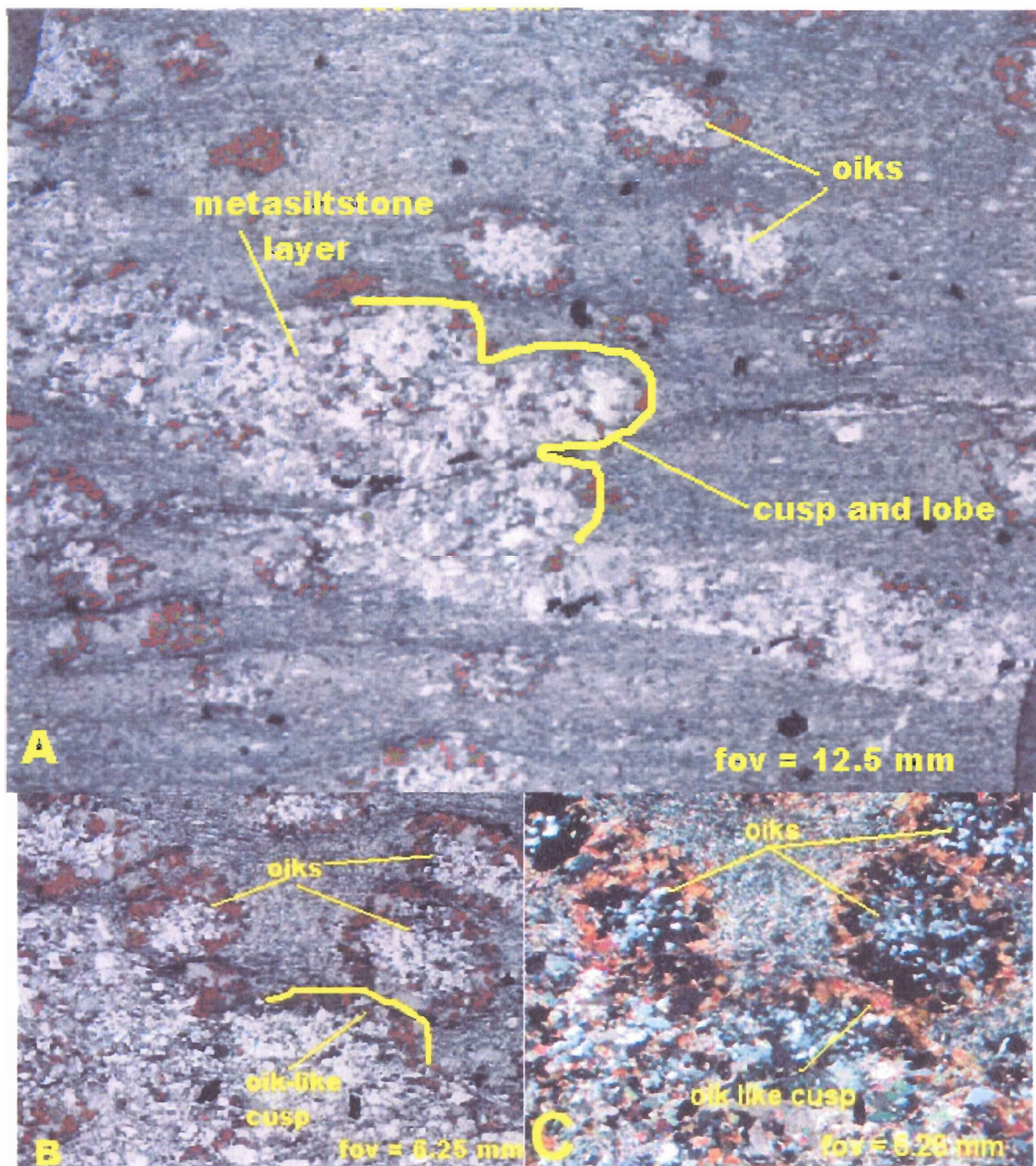
Figure 4.8: Sample M8 from Montague showing a folded metasiltstone layer surrounded by oikocrysts in A (PPL), and what resembles an oikocryst forming from the metasiltstone layer in B (PPL) and C (XN). Notice that the texture within the fully formed oikocrysts is similar to the metasiltstone texture. Plane of section is perpendicular to S_1 and $L_{oik.}$
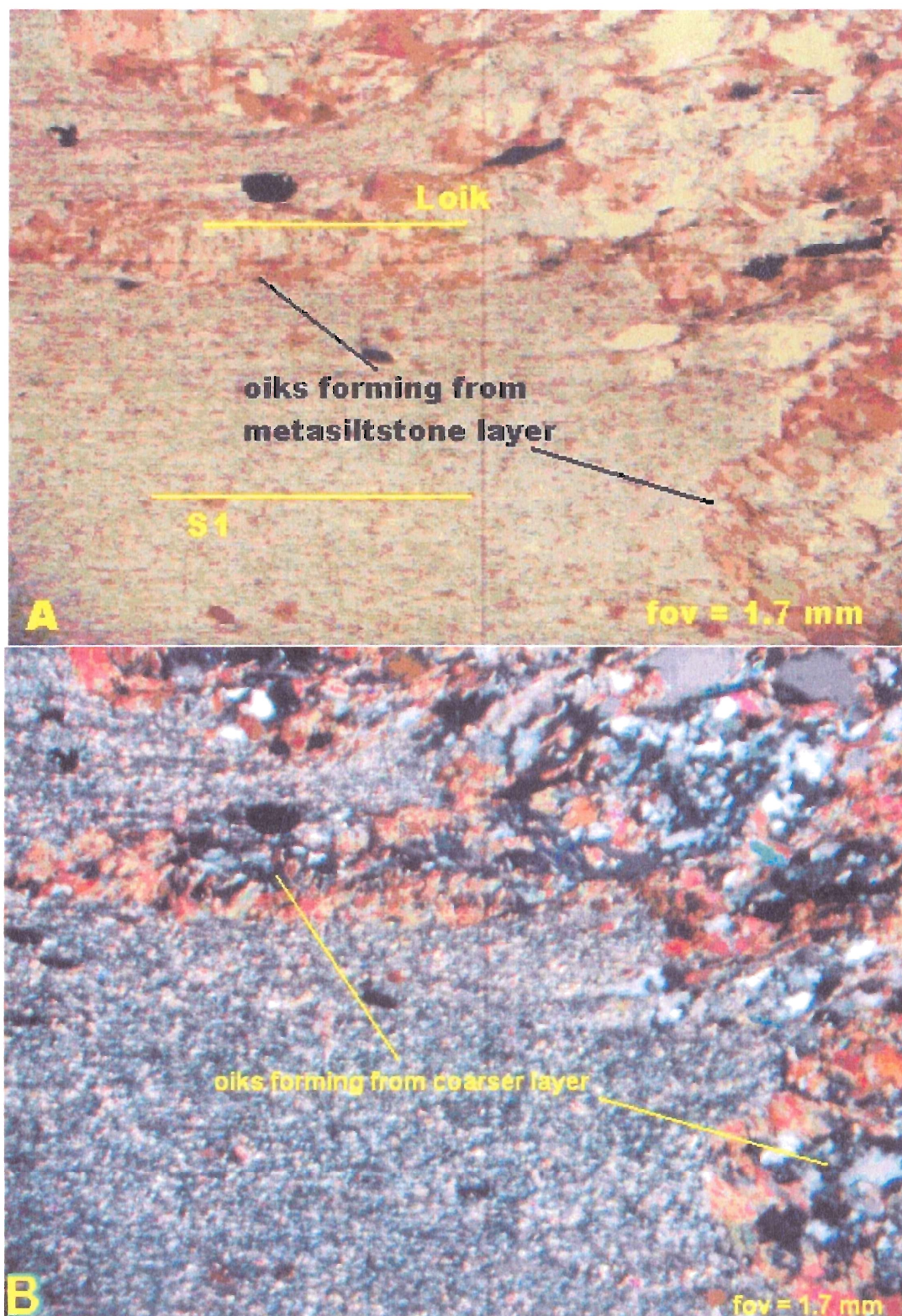
Figure 4.9: Sample M8 from Montague showing the contact between metasiltstone and slate, where microlithons have an interior texture similar to the metasiltstone. In PPL (A), and XN (B).
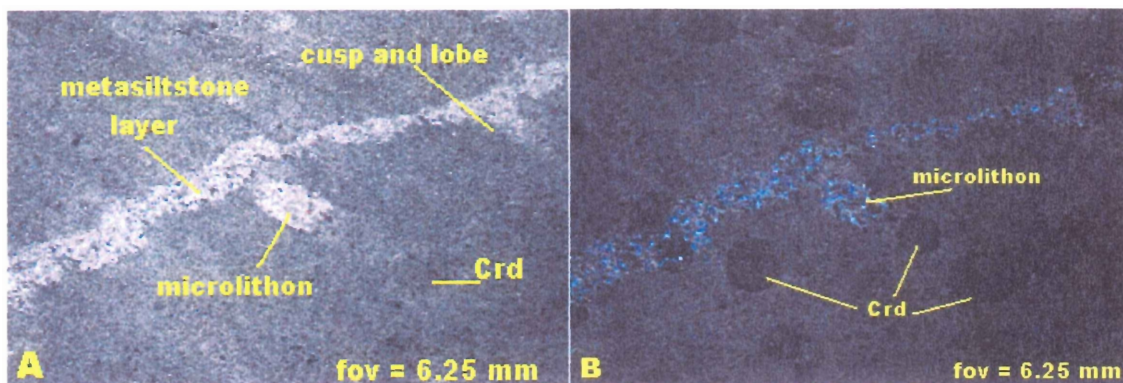
Figure 4.10: Sample PPP-20 from Point Pleasant Park in Halifax, NS, displaying a folded metasiltstone layer, displaying cusp and lobe structures. Both isolated microlithons and cordierite porphyroblasts are present (A) PPL; (B) XN

throughout the Meguma Group to determine whether the oikocrysts occur in any non-gold-bearing antiforms.

If oikocrysts are microlithons, significant local volume loss is implied. In order to link the volume loss necessary for the observed isolated microlithon distribution to the migration of material in the rock, geochemistry and mass balance calculations on the sulphides would be required, and the source of the sulphides would have to be determined geochemically. Geochemical analysis could also determine whether quartz was extracted from the rock and relocated to the veins, aiding the coarse-grained microlithons to form as isolated ellipsoidal oikocrysts in the matrix.

4.6 Summary of Results

It is obvious that the Goldenville Formation and especially the antiformal gold districts have experienced extensive folding as well as extensive hydrothermal activity. However it is still unknown what caused oikocrysts to form. From the hypotheses discussed in this chapter it seems as though the oikocryst formation is a result of high strain affecting metasiltstone layers in predominantly slaty matrix. This could have been

facilitated by the presence of hydrothermal fluids in the system. The question is whether the microlithons formed during the hydrothermal fluid migration through the deformed rocks, or whether they formed prior to hydrothermal activity. Cross-cutting veins suggest that the hydrothermal activity post-dates the oikocrysts. However, it may not post-date the rims. If oikocrysts were present prior to the hydrothermal activity, the rims that characterize oikocrysts may have formed during fluid migration through the rocks.

.

Chapter 5

CONCLUSIONS

The primary objectives of this thesis were to document oikocrysts and to test possible hypotheses for their origin. The three hypotheses that were explored were: firstly, oikocrysts originate from the alteration of cordierite; secondly, oikocrysts originate from the replacement of arsenopyrite; and thirdly, oikocrysts originate from isolated fragments (microlithons) of highly deformed metasiltstone layers.

Oikocrysts are ellipsoidal mineral aggregates in the slate and metasiltstone of the Goldenville Formation that are spatially related to gold districts. They form a down-dip lineation (L_1) on the cleavage plane and are perpendicular to antiformal fold hinges in the gold districts. They are classified into four types based on their rim and internal mineralogy and texture. Type I (BCC) is restricted to metasiltstone layers, and is only observed at Oldham and Montague. Type II (BCRO) is the most common, consisting intergrown biotite and chlorite rims with a core of granoblastic quartz, feldspar, and carbonate. These occur at most locations in both the slate and metasiltstone. Type III (CRO) is restricted to areas where there is less biotite in the matrix, and they have a chlorite-dominated rim and core. Type IV (BRO) is restricted to Mooseland where biotite also forms porphyroblasts in the matrix. At Mooseland and Montague, the oikocrysts and the matrix are overprinted by a later schistosity (S_2) defined by muscovite, biotite, and oxides oriented at an angle to the compositional layering foliation (S_1). This area is also affected by contact metamorphism.

After testing the three hypotheses through petrographic and microprobe analysis, the altered cordierite hypothesis was ruled out because the internal fabric of the oikocrysts does not resemble altered cordierite in terms of either mineralogy or texture.

The second hypothesis is viable for those cases where oikocrysts and sulphides occur together, i.e. Mooseland and Montague. Fine-grained, irregular, embayed pyrrhotite was observed within oikocrysts and in isolation in the matrix. Coarse-grained, idioblastic arsenopyrite porphyroblasts were observed in the cores of some of the oikocrysts hosting inclusions of fine-grained embayed sulphides. This suggests that pyrrhotite was being dissolved from the oikocryst cores during fluid migration, and was replaced by arsenopyrite.

The third hypothesis is viable throughout all the districts because it is based on the presence of both slate and metasiltstone of the Goldenville Formation. In samples where slate and metasiltstone were in contact, rimmed mineral aggregates grading from the buckled cusps of the metasiltstone layers resemble an early stage in the isolation of oikocrysts as microlithons in the slate matrix. The volume of metasiltstone lost during this process is not known; however, this hypothesis suggests that high amounts of strain and solution migration are required for oikocryst genesis.

With the results and observations thus far, a clear understanding of oikocryst origin is still unclear; however, it is impossible that it is a coincidence that oikocrysts are associated only with sulphide-rich anticlines in the Meguma terrane. The spatial relationship between oikocrysts and gold would be best described by combining the effects of high strain on the lithology with the sulphide dissolution and replacement through hydrothermal fluid migration. To determine whether sulphides are linked to

oikocrysts, geochemical data and mass balance calculations will be required in order to compare the sulphides-bearing oikocrysts with the oikocrysts containing no sulphides, and also to provide a chemical reaction that would support the migration of sulphides.

References

American Geological Institute. 1960. Glossary of Geology and Related Sciences. 2nd ed. The American Geological Institute, Washington, D.C.

Bates, J.L. 1987. Gold in Nova Scotia. Nova Scotia Department of Natural Resources, Mineral Resources Branch. Information Series ME 13. Available from http://www.gov.ns.ca/NATR/meb/is/is13.htm [cited 2003].

Boulter, M. C. 1989. Four dimensional analysis of geological maps. Structural Geology. Wiley.

Faribault, E. R. 1898. Plan and sections, Oldham Gold District, Halifax County, Nova Scotia. Geological Survey of Canada, Map 642, scale 1:6000.

Faribault, E.R. 1899. Plan and section, Mooseland Gold District, Halifax County, Nova Scotia. Geological Survey of Canada, Map 648, scale 1:3000.

Henderson, J.R., and Henderson, M.N. 1986. Constraints on the origin of gold in the Meguma Zone, Ecum Secum area, Nova Scotia. Maritime Sediments and Atlantic Geology, 22, p 1-14.

Hicks, R.J. 1996. Low-Grade Metamorphism in the Meguma Group, Southern Nova Scotia. B.Sc. Honours thesis, Department of Earth Sciences, Dalhousie University, Halifax, N.S.

Horne, R.J., Baker, D., Feetham, M., MacDonald, L. 1996. Preliminary Geology of the Waverley – Halifax Airport Area, Central Nova Scotia: Some Insights on the Timing of Deformation and Vein Formation in the Meguma Group. *In* Minerals and Energy Branch Report of Activities 1996. Edited by D.R. MacDonald and K.A. Mills. Nova Scotia Department of Natural Resources, Minerals and Energy Branch Report 97-1, p. 57-72.

Horne, R.J., Covey, G., Albert, C. 2003. Geological Report on the Early Stages of Development of the Mooseland Gold District (NTS 11D/15) Halifax County. In Minerals and Energy Branch Report of Activities 2003; Nova Scotia Department of Natural Resources, Report 2004-1, p. 25-39.

Horne, R.J., and Culshaw, N.G. 2001. Flexural slip folding in the Meguma Group, Nova Scotia, Canada. Fold development, veining and localization of gold deposits. Journal of Structural Geology, 23: 1631-1652.

Jamieson, R.A., Tobey, N. & ERTH 3020. 2005. Contact metamorphism of the Malifax Formation on the southeastern margin of the Halifax Pluton, Halifax, Nova Scotia. GAC-MAC-CSPG-CSSS Joint Annual Meeting, Halifax, NS, Abstracts, p. 95.

Keppie, J.D., 1976. Structural Model for the saddle reef and associated gold veins in the Meguma Group, Nova Scotia. Paper 76-1, Nova Scotia Department of Mines: a joint project with the Canada Department of Regional Economic Expansion.

Keppie, J.D., 1985. The Appalachian collage in Gee, D. G. and Stuart, B.A., eds, The Caledonian Orogen – Scandinavia and related areas: John Wiley and Sons, Chichester, U.K, p. 422-437.

Keppie, J.D. and Muecke, G.K. 1979. Metamorphic Map of Nova Scotia, [1:1 000 000]. Nova Scotia Department of Natural resources, Mineral Resources Branch.

Keppie, D.F., Keppie, J.D., and Murphy, J.B. 2002. Saddle reef auriferous veins in a conical fold termination (Oldham anticline, Meguma Terrane, Nova Scotia, Canada): reconciliation of structural and age data. Canadian Journal of Earth Sciences, 39, p. 53-63.

Kontak, D.J. and Smith P.K. 1990. Geological and $^{40}Ar/^{39}Ar$ geochronological constraints on the timing of quartz vein formation in the Meguma Group lode-gold deposits, Nova Scotia. Atlantic Geology, 26, p. 201-227.

Kontak, D.J., Smith, P.K., Kerrich, R., and Williams, P.F., 1990. Integrated model for Meguma Group lode gold deposits, Nova Scotia, Canada. Geology, 18: 238-242

MacDonald, L.A. 1998. Carbonate in the Oldham Gold Deposit, Nova Scotia. B.Sc. Honours thesis, Department of Earth Sciences, Dalhousie University, Halifax, N.S.

MacDonald, M.A., and O'Reilly, G.A. 1989. Gold enrichment associated with post-magmatic processes in the South Mountain Batholith, southwestern Nova Scotia. Nova Scotia Department of Mines and Energy, Report 89-1, p. 13-26

Malcolm, W. 1929. Gold Fields of Nova Scotia. Geological Survey of Canada, Memoir 385. p. 124.

Melvin, A.E. 1987. Vein-Host Rock Relationships in the Mooseland Gold District of the Meguma Group, Nova Scotia. B.Sc. Honours thesis. Department of Earth Sciences. Saint Francis Xavier University, Antigonish, N.S.

Nova Scotia Department of Natural Resources. 1976. Geology Minerals and Mining in Nova Scotia [Online]. Mineral Resources Branch, Department of Natural Resources, Province of Nova Scotia. Information Series ME 1. Available from http://www.gov.ns.ca/natr/meb/is/is01.htm [cited 21 June 2006]

Sangster, A.L. and Smith, P.K. 2006. Mineral Deposits of Canada, Metallogenic Summary, Meguma Gold Deposits [Online]. Geological Survey of Canada and The Mineral Deposits Division of the Geological Association of Canada. Available from

Inhttp://gsc.nrcan.gc.ca/mindep/metallogeny/gold/meguma/index_e.php [cited 18 April 2006] "In Press"

Smith, P.K. and Kontak, D.J. 1988. Meguma gold studies I: generalized geological aspects of the Beaver Dam gold deposit, eastern Meguma zone, Nova Scotia. *In* Mines and Minerals Branch Report of Activities 1987, Part B. Edited by D. R. MacDonald and K. A. Mills. Nova Scotia Department of Mines and Energy Report 88-1, p. 45-59.

Smith, P.K. and Kontak, D.J. 1996. Gold Deposits in the Meguma Group of Nova Scotia. Nova Scotia Department of Natural Resources Minerals and Energy Branch. Information Circular 51

Twiss, R.J. and Moores, E.M. 1992. Structural Geology. W. H. Freeman and Company, University of California, California.

White, C.E. 2003. Preliminary Bedrock Geology of the Area Between Chebogue Point, Yarmouth County, and Cape Sable Island, Shelburne County, Southwestern Nova Scotia. *In* Minerals Branch Report of Activities 2002; Nova Scotia Department of Natural Resources, Report 2003-1, p. 127-145.

White, C.E., Horne, R.J., and Barr, S.M. 2007. The Meguma Group of southern Nova Scotia: new insights on the stratigraphy, tectonic setting, and provenance. Atlantic Geoscience Society Annual General Meeting 2007, Moncton, NB, Abstracts. p. 42.

Wood, D.S. 1974. Current Views of the Development of Slaty Cleavage. Department of Geology, University of Illinois, Urbana, Illinois.

Appendix A: Microprobe data

For sample locations, refer to Appendix B, Fig 2.1, and Fig 2.2.

Table A.1: Muscovite

Slide-Area	o1-b-A2	o1-b-A2	o1-b-A2	o1-b-A3	o1-b-A3	o1-b-A3	o1-b-A3	o1-b-A4	o1-b-A4	m-2-A	o1-b-A4
Point #	3	16	17	2	3	7	17	6	10	9	11
SiO2	47.15	46.48	47.73	45.73	49.03	44.84	47.42	47.70	46.79	47.71	47.87
Al2O3	33.32	31.12	34.25	31.55	32.33	34.62	33.90	33.08	33.38	30.96	33.73
Cr2O3	0.00	0.01	0.00	0.00	0.00	0.00	0.00	0.00	0.00	0.02	0.00
FeO	2.53	3.41	2.15	4.41	2.55	3.05	2.60	2.68	2.44	4.20	2.40
MgO	1.29	1.82	1.08	2.25	1.80	0.70	1.36	1.55	1.45	1.99	1.42
CaO	0.00	0.00	0.00	0.00	0.00	0.03	0.00	0.00	0.00	0.15	0.00
Na2O	0.30	0.17	0.32	0.16	0.19	0.46	0.25	0.19	0.23	0.20	0.13
K2O	9.52	10.01	10.09	9.04	9.17	9.83	10.18	10.32	9.86	9.91	7.36
TiO2	0.39	0.41	0.37	0.97	0.21	1.00	0.41	0.43	0.25	0.36	0.23
MnO	0.01	0.00	0.00	0.00	0.00	0.00	0.00	0.00	0.00	0.04	0.00
Total	94.52	93.43	95.99	94.12	95.28	94.54	96.12	95.95	94.40	95.54	93.16
					Cations corrected to 11 Oxygens						
Si	3.16	3.18	3.15	3.11	3.24	3.03	3.14	3.16	3.14	3.20	3.20
Ti	0.02	0.02	0.02	0.05	0.01	0.05	0.02	0.02	0.01	0.02	0.01
Al	2.63	2.51	2.66	2.53	2.52	2.76	2.64	2.59	2.64	2.45	2.66
Fe	0.14	0.19	0.12	0.25	0.14	0.17	0.14	0.15	0.14	0.24	0.13
Mg	0.13	0.19	0.11	0.23	1.77	0.07	0.13	0.15	0.15	0.20	0.14
Na	0.04	0.02	0.04	0.02	0.02	0.06	0.03	0.02	0.03	0.03	0.02
K	0.81	0.87	0.85	0.79	0.77	0.85	0.86	0.87	2.30	0.85	0.63
Cation Total	6.93	6.99	6.95	6.98	6.89	6.99	6.97	6.97	6.96	6.99	6.79

Slide-Area	m8-c-a3	m8-c-a3	m8-c-a2-a	m8-c-a2-a	m8-c-a2-a	m8-c-a2-b	m8-c-a2-b	m8-c-a2-b	o4-a1	o4-a1
Point #	3	8	8	14	15	7	9	10	6	9
SiO2	46.15	45.93	48.00	48.15	47.32	48.75	47.47	49.03	48.60	48.94
Al2O3	34.44	34.12	34.11	33.57	33.47	34.25	31.44	31.82	32.35	30.86
Cr2O3	0.00	0.00	0.00	0.00	0.00	0.00	0.00	0.00	0.00	0.00
FeO	3.09	2.42	2.08	2.72	2.82	2.44	2.65	2.49	2.57	2.98
MgO	0.82	0.88	1.23	1.18	1.31	1.30	1.75	1.88	1.73	2.10
CaO	0.00	0.00	0.00	0.00	0.00	0.00	0.00	0.00	0.00	0.00
Na2O	0.68	0.41	0.20	0.36	0.23	0.19	0.10	0.08	0.25	0.20
K2O	2.02	8.52	0.10	8.34	0.00	0.00	0.00	0.00	1.99	0.02
TiO2	0.44	0.12	0.25	0.09	0.24	0.07	0.07	0.02	0.49	0.13
MnO	0.00	0.04	0.00	0.00	0.00	0.00	0.00	0.00	0.00	0.00
Total	95.16	93.98	95.65	96.08	95.65	96.85	93.14	94.65	96.09	95.49
				Cations corrected to 11 Oxygens						
Si	3.09	3.11	3.17	3.18	3.15	3.18	3.23	3.26	3.21	3.26
Ti	0.02	0.01	0.01	0.00	0.01	0.00	0.00	0.00	0.02	0.01
Al	0.27	2.83	2.65	2.61	2.63	2.63	2.52	2.50	2.52	2.42
Fe	0.17	0.14	0.12	0.15	0.16	0.13	0.15	0.14	0.14	0.17
Mg	0.08	0.09	0.12	0.12	0.13	0.13	0.18	0.19	0.17	0.21
Na	0.09	0.05	0.03	0.05	0.03	0.02	0.01	0.01	0.03	0.03
K	8.14	0.87	0.82	0.84	8.71	0.82	0.84	0.79	0.85	0.87
Cation Total	6.98	6.99	6.92	6.95	6.98	6.92	6.93	6.88	6.95	6.97

Slide-Area	o4-a1	o4-a1	o4-a1	old-6b-a2	old-6b-a2	old-6b-a2-b	ml-51a-a	ml-51a-a	ml-51a-a-b	ml-51a-a-b
Point #	12	13	15	4	8	1	2	10	6	9
SiO2	47.92	47.68	47.80	48.94	47.45	45.44	48.39	46.81	48.70	45.66
Al2O3	33.04	32.98	31.16	31.03	33.10	36.18	36.86	33.28	32.57	36.08
Cr2O3	0.00	0.00	0.00	0.00	0.00	0.00	0.00	0.00	0.00	0.01
FeO	2.59	2.40	2.89	2.91	2.21	1.54	1.33	1.40	1.41	1.22
MgO	1.55	1.45	1.72	2.01	1.38	0.50	1.01	1.46	1.86	0.90
CaO	0.00	0.00	0.00	0.00	0.00	0.00	0.01	0.07	0.00	0.03
Na2O	0.25	0.29	0.52	0.25	0.26	1.10	0.35	0.22	0.23	0.36
K2O	0.03	10.09	0.05	10.25	0.07	0.04	0.07	0.01	9.29	9.19
TiO2	0.36	0.48	0.53	0.32	0.45	0.78	0.08	0.78	0.38	0.16
MnO	0.00	0.00	0.00	0.00	0.00	0.00	0.02	0.00	0.03	0.02
Total	95.98	95.53	94.73	95.96	94.85	94.85	97.89	94.39	95.45	94.40
					Cations corrected to 11 Oxygens					
Si	3.17	3.17	3.22	3.25	3.17	3.03	3.11	3.14	3.22	3.05
Ti	0.02	0.02	0.03	0.02	0.02	0.04	0.00	0.04	0.02	0.01
Al	2.58	2.59	2.47	2.43	2.61	2.84	2.79	2.63	2.54	2.84
Fe	0.14	0.13	0.16	0.16	0.12	0.09	0.07	0.08	0.08	0.07
Mg	0.15	0.14	0.17	0.20	0.14	0.05	0.10	0.15	0.18	0.09
Na	0.03	0.04	0.07	0.03	0.03	0.14	0.04	0.03	0.03	0.05
K	0.87	0.87	0.87	0.89	0.85	0.79	0.81	0.89	0.87	0.85
Cation Total	6.97	6.97	6.99	6.98	6.95	6.98	6.92	6.96	6.94	6.96

Slide-Area	OLD-6-c	OLD-6-c	ML-50-b	ML-50-b	ML-50-b	ML-50-b	ML-50-a	ML-50-a	ML-50-a
Point #	7	13	3	6	10	12	8	17	18
SiO2	47.63	46.85	46.28	47.02	46.04	45.46	45.57	45.91	47.82
Al2O3	31.87	32.93	35.91	33.64	35.96	36.10	35.64	36.30	33.78
Cr2O3	0.01	0.04	0.00	0.00	0.00	0.00	0.00	0.00	0.00
FeO	2.75	3.01	1.16	1.22	1.43	1.08	1.13	1.14	1.35
MgO	1.73	1.53	0.84	1.28	0.99	0.75	0.78	0.86	1.43
CaO	0.01	0.02	0.00	0.00	0.00	0.00	0.00	0.00	0.00
Na2O	0.20	0.29	0.42	0.31	0.44	0.41	0.43	0.43	0.27
K2O	0.11	6.39	0.16	0.02	10.14	0.00	9.01	8.88	0.10
TiO2	0.53	0.46	0.00	0.42	0.00	0.00	0.00	0.00	0.31
MnO	0.01	0.02	0.00	0.00	0.00	0.00	0.00	0.00	0.00
Total	95.06	95.42	94.75	94.00	95.00	93.99	93.65	94.76	95.18
					Cations corrected to 11 Oxygens				
Si	3.19	3.14	3.08	3.16	3.06	3.05	3.07	3.06	3.17
Ti	0.03	0.02	0.00	0.02	0.00	0.00	0.00	0.00	0.02
Al	2.52	2.60	2.82	2.66	2.82	2.86	2.83	2.85	2.64
Fe	0.15	0.17	0.06	0.07	0.08	0.06	0.06	0.06	0.07
Mg	0.17	0.15	0.08	0.13	0.10	0.08	0.08	0.08	1.41
Na	0.03	0.04	0.05	0.04	0.06	0.05	0.06	0.06	0.04
K	0.88	0.88	0.86	0.87	0.86	0.87	0.87	0.86	0.86
Cation Total	6.98	7.00	6.97	6.94	6.98	6.98	6.97	6.97	6.94

Table A.2: Biotite

Slide-Area	o1-b-A2	o1-b-A2	o1-b-A2	o1-b-A2	o1-b-A2	o1-b-A2	o1-b-A2	o1-b-A3	o1-b-A3	o1-b-A3
Point #	1	5	11	14	15	18	20	1	11	13
SiO2	35.81	35.08	34.67	35.63	34.85	35.76	35.41	36.56	36.49	35.49
Al2O3	17.65	17.74	17.47	17.30	17.06	17.27	18.20	17.54	17.78	17.49
Cr2O3	0.03	0.07	0.05	0.05	0.05	0.04	0.03	0.04	0.01	0.01
FeO	22.54	22.55	23.23	22.54	22.60	22.19	22.60	23.06	22.63	22.72
MgO	8.05	8.02	8.37	8.18	7.90	8.19	7.98	8.28	8.33	8.22
CaO	0.00	0.00	0.00	0.00	0.00	0.00	0.00	0.00	0.07	0.00
Na2O	0.01	0.03	0.01	0.03	0.01	0.04	0.02	0.03	0.03	0.02
K2O	8.25	8.41	7.58	8.43	8.35	8.41	8.47	8.52	8.45	8.48
TiO2	2.11	1.97	2.12	2.00	2.10	2.29	2.04	2.11	2.14	1.99
MnO	0.14	0.17	0.15	0.13	0.13	0.17	0.14	0.14	0.12	0.14
Total	94.59	94.06	93.67	94.29	93.07	94.37	94.90	96.28	96.05	94.58
					Cations corrected to 11 Oxygens					
Si	2.77	2.74	2.72	2.77	2.75	2.77	2.73	2.78	2.78	2.75
Ti	0.12	0.12	0.13	0.12	0.12	0.13	0.12	0.12	0.12	0.12
Al	1.61	1.63	1.61	1.59	1.59	1.58	1.66	1.57	1.60	1.60
Fe	1.46	1.47	1.52	1.47	1.49	1.44	1.46	1.47	1.44	1.48
Mg	0.93	0.93	0.98	0.95	0.93	0.95	0.92	0.94	0.94	0.95
K	0.81	0.84	0.76	0.84	0.84	0.83	0.83	0.83	0.82	0.84
Cation Total	7.71	7.75	7.73	7.74	7.75	7.72	7.74	7.73	7.72	7.75
Mol% Annite	61.09	61.21	60.92	60.71	61.62	60.30	61.38	60.97	60.38	60.79
Mol% Phlogopite	38.91	38.79	39.08	39.29	38.38	39.70	38.62	39.03	39.62	39.21

Mol% Annite = Fe/(Fe+Mg)x100%; Mol% Phlogopite = Mg/(Fe+Mg)x100%

Slide-Area	o1-b-A3	o1-b-A4	o1-b-A4	m-2-A	o1-b-A4	m8-c-a3	m8-c-a3	m8-c-a3	m8-c-a3	m8-c-a3	m8-c-a3
Point #	15	3	8	6	4	4	7	9	12	15	17
SiO2	35.87	35.34	35.79	35.75	35.78	35.65	34.77	35.60	37.03	36.74	36.57
Al2O3	18.01	18.46	17.82	18.08	31.73	17.86	17.56	18.10	17.32	18.13	17.36
Cr2O3	0.02	0.06	0.01	0.06	0.00	0.03	0.05	0.06	0.07	0.05	0.04
FeO	23.27	23.69	23.17	22.34	8.94	22.28	22.33	22.84	21.93	22.04	21.85
MgO	8.24	7.89	8.44	8.75	6.21	8.48	8.61	8.56	9.10	9.02	8.84
CaO	0.05	0.00	0.00	0.00	0.30	0.00	0.03	0.01	0.03	0.06	0.06
Na2O	0.06	0.04	0.03	0.08	2.48	0.00	0.02	0.02	0.00	0.03	0.01
K2O	8.37	8.19	8.17	8.19	0.05	8.52	8.24	8.43	8.49	7.88	7.97
TiO2	2.15	1.89	2.12	2.21	1.08	1.98	1.97	1.79	2.09	2.09	2.09
MnO	0.14	0.14	0.13	0.17	0.00	0.23	0.18	0.20	0.19	0.19	0.19
Total	96.17	95.70	95.69	95.64	86.55	95.02	93.75	95.60	96.26	96.22	94.99
Cations corrected to 11 Oxygens											
Si	2.74	2.71	2.74	2.73	2.65	2.75	2.72	2.73	2.80	2.77	2.80
Ti	0.12	0.11	0.12	0.13	0.06	0.11	0.12	0.10	0.12	0.12	0.12
Al	1.62	1.67	1.61	1.63	2.77	1.62	1.62	1.64	1.54	1.61	1.57
Fe	1.49	1.52	1.48	1.43	0.55	1.44	1.46	1.47	1.39	1.39	1.40
Mg	0.94	0.90	0.96	1.00	6.84	0.97	1.00	0.98	1.03	1.01	1.01
K	0.01	0.80	0.80	0.80	0.01	0.84	0.82	0.83	0.82	0.76	0.78
Cation Total	7.74	7.74	7.73	7.73	7.09	7.75	7.76	7.76	7.72	7.69	7.69
Mol% Annite	61.31	62.77	60.63	58.87	7.47	59.59	59.28	59.97	57.47	57.80	58.12
Mol% Phlogopite	38.69	37.23	39.37	41.13	92.53	40.41	40.72	40.03	42.53	42.20	41.88

Mol% Annite = Fe/(Fe+Mg)x100%; Mol% Phlogopite = Mg/(Fe+Mg)x100%

Slide-Area	m8-c-a3	m8-c-a3	m8-c-a3-b	m8-c-a3-b	m8-c-a2-a	m8-c-a2-a	m8-c-a2-a	m8-c-a2-a	m8-c-a2-b
Point #	18	20	6	8	3	7	10	13	2
SiO2	38.02	35.98	36.33	37.41	35.86	35.57	36.30	37.00	35.07
Al2O3	17.13	17.72	17.74	17.64	17.66	18.01	17.02	18.13	17.40
Cr2O3	0.05	0.01	0.05	0.06	0.03	0.00	0.00	0.00	0.00
FeO	21.22	21.41	21.55	21.78	22.17	21.76	21.79	21.71	22.22
MgO	8.74	8.62	8.72	8.96	8.66	8.59	8.82	8.92	8.92
CaO	0.02	0.03	0.01	0.02	0.00	0.00	0.00	0.00	0.00
Na2O	0.00	0.00	0.00	0.05	0.00	0.00	0.00	0.00	0.00
K2O	8.28	8.48	8.48	8.21	8.51	8.03	8.34	8.04	8.20
TiO2	2.03	1.82	2.08	2.07	2.13	1.85	1.99	1.95	1.99
MnO	0.17	0.18	0.20	0.16	0.19	0.05	0.06	0.06	0.05
Total	95.66	94.25	95.16	96.36	95.20	93.85	94.33	95.81	93.85
Cations corrected to 11 Oxygens									
Si	2.87	2.78	2.78	2.81	2.75	2.76	2.80	2.80	2.74
Ti	0.12	0.11	0.12	0.12	0.12	0.11	0.12	0.11	0.12
Al	1.52	1.61	1.60	1.56	1.60	1.65	1.55	1.61	1.60
Fe	1.34	1.38	1.38	1.37	1.42	1.41	1.41	1.37	1.45
Mg	0.98	0.99	0.99	1.01	0.99	0.99	1.02	1.00	1.04
K	0.80	0.84	0.83	0.79	0.83	0.79	0.82	0.77	0.82
Cation Total	7.65	7.73	7.71	7.68	7.74	7.71	7.72	7.67	7.76
Mol% Annite	57.64	58.19	58.09	57.69	58.95	58.70	58.10	57.73	58.32
Mol% Phlogopite	42.36	41.81	41.91	42.31	41.05	41.30	41.90	42.27	41.68

Mol% Annite = Fe/(Fe+Mg)x100%; Mol% Phlogopite = Mg/(Fe+Mg)x100%

Slide-Area	m8-c-a2-b	m8-c-a2-b	m8-c-a2-b	m8-c-a2-b	m8-c-a2-b	old-6b-a2	old-6b-a2	old-6b-a2-b
Point #	11	15	16	18	19	6	10	2
SiO2	38.31	36.54	35.54	35.00	35.76	35.92	32.94	34.09
Al2O3	16.63	17.69	18.09	17.84	17.74	17.40	16.83	17.48
Cr2O3	0.00	0.00	0.00	0.00	0.00	0.06	0.02	0.03
FeO	20.74	21.83	21.96	21.68	22.06	22.32	23.28	24.46
MgO	9.65	8.77	8.60	8.72	8.68	8.63	8.55	9.57
CaO	0.00	0.00	0.00	0.00	0.00	0.01	0.04	0.01
Na2O	0.00	0.00	0.00	0.00	0.00	0.02	0.03	0.01
K2O	8.15	8.17	8.19	7.92	8.11	8.20	7.91	6.65
TiO2	2.08	1.92	1.86	1.81	1.91	2.02	2.02	1.52
MnO	0.03	0.04	0.06	0.04	0.04	0.10	0.13	0.11
Total	95.59	94.96	94.30	93.02	94.30	94.68	91.74	93.92
Cations corrected to 11 Oxygens								
Si	2.88	2.80	2.75	2.74	2.76	2.77	2.66	2.67
Ti	0.12	0.11	0.11	0.11	0.11	0.12	0.12	0.09
Al	1.48	1.59	1.65	1.65	1.62	1.58	1.60	1.61
Fe	1.31	1.40	1.42	1.42	1.43	1.44	1.57	1.60
Mg	1.08	1.00	0.99	1.02	1.00	0.99	1.03	1.12
K	0.78	0.80	0.81	0.79	0.80	0.81	0.82	0.66
Cation Total	7.65	7.70	7.73	7.73	7.72	7.72	7.82	7.77
Mol% Annite	54.68	58.24	58.90	58.23	58.78	59.20	60.41	58.92
Mol% Phlogopite	45.32	41.76	41.10	41.77	41.22	40.80	39.59	41.08

Mol% Annite = Fe/(Fe+Mg)x100%; Mol% Phlogopite = Mg/(Fe+Mg)x100%

Slide-Area	ML-50-b	ML-50-b	ML-50-b	ML-50-a	ML-50-a	ML-50-a	ML-50-a	ML-50-a	ML-50-a
Point #	4	9	11	1	5	10	14	16	20
SiO2	35.98	35.73	35.10	35.84	34.61	35.11	34.89	36.20	35.40
Al2O3	18.72	19.94	20.43	18.81	18.61	18.77	18.89	18.31	18.76
Cr2O3	0.00	0.00	0.00	0.00	0.00	0.00	0.00	0.00	0.00
FeO	20.13	19.03	18.76	20.03	20.04	19.53	20.23	19.97	19.38
MgO	9.65	9.76	9.62	9.51	9.02	9.43	8.84	9.54	9.22
CaO	0.00	0.00	0.00	0.00	0.00	0.00	0.00	0.04	0.00
Na2O	0.05	0.06	0.08	0.06	0.08	0.07	0.08	0.06	0.06
K2O	9.04	9.18	8.99	9.01	8.86	8.88	8.95	8.86	8.79
TiO2	2.09	1.17	1.38	2.03	1.91	2.08	2.16	2.10	2.11
MnO	0.26	0.23	0.24	0.22	0.27	0.24	0.28	0.23	0.22
Total	95.91	95.11	94.59	95.50	93.39	94.12	94.33	95.32	93.93
Cations corrected to 11 Oxygens									
Si	2.72	2.71	2.67	2.72	2.70	2.70	2.69	2.75	2.72
Ti	0.12	0.07	0.08	0.12	0.11	0.12	0.13	0.12	0.12
Al	1.67	1.78	1.83	1.68	1.71	1.70	1.72	1.64	1.70
Fe	1.27	1.21	1.19	1.27	1.31	1.26	1.31	1.27	1.25
Mg	1.09	1.10	1.09	1.08	1.05	1.08	1.02	1.08	1.06
K	0.87	0.89	0.87	0.87	0.88	0.87	0.99	0.09	0.86
Cation Total	7.77	7.78	7.77	7.76	7.78	7.77	7.77	7.74	7.74
Mol% Annite	53.91	52.24	52.24	54.15	55.47	53.74	56.23	54.00	54.13
Mol% Phlogopite	46.09	47.76	47.76	45.85	44.53	46.26	43.77	46.00	45.87

Mol% Annite = Fe/(Fe+Mg)x100%; Mol% Phlogopite = Mg/(Fe+Mg)x100%

Table A.3: Chlorite

Slide-Area	o1-b-A2	o1-b-A2	o1-b-A2	o1-b-A2	o1-b-A2	o1-b-A2	o1-b-A3	o1-b-A3	o1-b-A3	o1-b-A3	o1-b-A4
Point #	2	7	9	10	13	19	6	10	16	18	1
SiO2	23.26	24.80	24.10	25.09	24.14	24.72	24.55	24.65	25.17	23.05	25.37
Al2O3	22.09	20.37	21.58	20.60	21.83	21.53	21.95	21.09	21.93	21.50	22.28
Cr2O3	0.04	0.01	0.03	0.03	0.05	0.00	0.00	0.01	0.00	0.01	0.02
FeO	29.59	28.80	28.36	28.78	29.29	28.96	29.38	29.69	29.75	28.66	29.29
MgO	11.30	12.42	11.88	12.06	11.37	12.56	11.87	11.68	12.00	11.01	12.21
CaO	0.01	0.01	0.00	0.01	0.01	0.01	0.03	0.18	0.00	0.01	0.02
Na2O	0.00	0.00	0.00	0.00	0.00	0.01	0.01	0.00	0.00	0.00	0.00
K2O	0.06	0.02	0.01	0.52	0.06	0.09	0.09	0.02	0.06	0.09	0.05
TiO2	0.07	0.05	0.05	0.17	0.07	0.07	0.10	0.06	0.02	0.14	0.08
MnO	0.31	0.33	0.30	0.29	0.30	0.32	0.30	0.26	0.28	0.30	0.30
Total	86.73	86.81	86.30	87.54	87.12	88.27	88.29	87.62	89.21	84.77	89.62
Cations corrected to 28 Oxygens											
Si	5.10	5.40	5.27	5.42	5.25	5.29	5.26	5.34	5.33	5.16	5.33
Ti	0.01	0.01	0.01	0.03	0.01	0.01	0.02	0.01	0.00	0.03	0.01
Al	5.71	5.23	5.56	5.25	5.59	5.43	5.54	5.38	5.47	5.68	5.52
Fe	5.43	5.24	5.18	5.20	5.33	5.18	5.26	5.38	5.27	5.37	5.15
Mn	0.06	0.06	0.06	0.05	0.06	0.59	0.06	0.05	0.05	0.06	0.05
Mg	3.70	4.03	3.87	3.89	3.68	4.01	3.79	3.77	3.79	3.68	3.82
K	0.02	0.01	0.00	0.14	0.02	0.03	0.03	0.01	0.02	0.03	0.01
Cation Total	20.04	19.98	19.95	19.99	19.95	20.00	19.97	19.97	19.94	19.99	19.91
Xfe	0.59	0.57	0.57	0.57	0.59	0.56	0.58	0.59	0.58	0.59	0.57
XMg	0.41	0.43	0.43	0.43	0.41	0.44	0.42	0.41	0.42	0.41	0.43

Slide-Area	o1-b-A4	o1-b-A4	m-2-A	m-2-A	m-2-A	m-2-A	m-2-A	m-2-A	m-2-A	m-2-A	m8-c-a3	m8-c-a3
Point #	5	7	3	8	11	12	13	14	15	16	2	5
SiO2	24.76	26.49	25.31	24.86	26.03	24.14	25.20	25.04	26.98	25.11	25.39	24.71
Al2O3	21.60	21.70	22.94	21.50	22.54	21.25	22.82	22.92	22.31	21.48	21.17	22.56
Cr2O3	0.02	0.01	0.11	0.08	0.08	0.08	0.07	0.11	0.08	0.07	0.02	0.05
FeO	29.55	28.26	28.57	28.67	28.06	27.60	28.69	28.69	27.60	30.33	28.50	28.72
MgO	11.99	12.42	12.93	13.17	13.73	12.73	13.03	12.58	13.34	11.63	13.33	12.56
CaO	0.02	0.00	0.06	0.08	0.03	0.00	0.01	0.02	0.05	0.22	0.02	0.02
Na2O	0.00	0.18	0.04	0.04	0.06	0.04	0.05	0.05	0.07	0.04	0.00	0.00
K2O	0.06	0.05	0.05	0.04	0.04	0.07	0.04	0.06	0.59	0.04	0.03	0.07
TiO2	0.04	0.07	0.15	0.12	0.13	0.09	0.12	0.14	0.24	0.12	0.02	0.05
MnO	0.23	0.26	0.24	0.32	0.30	0.30	0.28	0.29	0.24	0.24	0.34	0.34
Total	88.26	89.44	90.39	88.87	91.00	86.30	90.30	89.90	91.51	89.28	88.83	89.09
					Cations corrected to 28 Oxygens							
Si	5.31	5.53	5.25	5.27	5.34	5.26	5.24	5.23	5.49	5.34	5.37	5.22
Ti	0.01	0.01	0.03	0.02	0.02	0.02	0.02	0.02	0.04	0.02	0.00	0.01
Al	5.46	5.34	5.61	5.37	5.45	5.46	5.59	5.64	5.35	5.38	5.28	5.62
Fe	5.30	4.94	4.95	5.08	4.81	5.03	4.98	5.01	4.70	5.39	5.05	5.07
Mn	0.04	0.05	0.04	0.06	0.05	0.05	0.05	0.05	0.04	0.04	0.06	0.06
Mg	3.83	3.87	4.00	4.16	4.20	4.14	4.03	3.92	4.05	3.69	4.21	3.96
K	0.02	0.01	0.01	0.01	0.01	0.02	0.01	0.02	0.15	0.01	0.01	0.02
Cation Total	19.96	19.83	19.93	20.03	19.93	20.01	19.96	19.93	19.88	19.96	19.96	19.97
Xfe	0.58	0.56	0.55	0.55	0.53	0.55	0.55	0.56	0.54	0.59	0.55	0.56
XMg	0.42	0.44	0.45	0.45	0.47	0.45	0.45	0.44	0.46	0.41	0.45	0.44

Slide-Area	m8-c-a3	m8-c-a3	m8-c-a3-b	m8-c-a3-b	m8-c-a3-b	m8-c-a3-b	m8-c-a2-a	m8-c-a2-b	m8-c-a2-b
Point #	11	16	1	2	7	11	4	3	6
SiO2	24.47	26.51	24.23	24.03	24.29	25.86	24.57	24.71	25.48
Al2O3	22.65	20.97	22.29	21.98	22.43	20.97	21.81	21.39	20.90
Cr2O3	0.05	0.05	0.06	0.02	0.03	0.04	0.05	0.00	0.00
FeO	28.74	27.67	28.19	28.80	28.49	27.59	28.45	28.28	27.88
MgO	12.51	13.20	12.54	12.49	12.47	13.69	12.65	13.22	13.72
CaO	0.02	0.01	0.02	0.02	0.01	0.01	0.00	0.00	0.00
Na2O	0.00	0.00	0.00	0.00	0.00	0.00	0.00	0.00	0.00
K2O	0.03	0.10	0.06	0.04	0.04	0.40	0.10	0.00	0.00
TiO2	0.05	0.10	0.06	0.04	0.06	0.05	0.09	0.00	0.00
MnO	0.36	0.34	0.35	0.34	0.34	0.34	0.35	0.16	0.20
Total	88.89	88.95	87.82	87.77	88.16	88.59	88.07	87.77	88.18
				Cations corrected to 28 Oxygens					
Si	5.18	5.56	5.19	5.17	5.19	5.45	5.26	5.29	5.41
Ti	0.01	0.02	0.01	0.01	0.01	0.01	0.01	0.00	0.00
Al	5.66	5.19	5.63	5.58	5.65	5.21	5.50	5.40	5.23
Fe	5.09	4.85	5.05	5.19	5.09	4.87	5.09	5.07	4.95
Mn	0.06	0.06	0.06	0.06	0.06	0.06	0.06	0.03	0.04
Mg	3.95	4.13	4.01	4.01	3.97	4.31	4.03	4.22	4.34
K	0.01	0.03	0.02	0.01	0.01	0.01	0.03	0.00	0.00
Cation Total	19.98	19.84	19.99	20.03	19.98	19.93	19.99	20.01	19.97
Xfe	0.56	0.54	0.56	0.56	0.56	0.53	0.56	0.55	0.53
XMg	0.44	0.46	0.44	0.44	0.44	0.47	0.44	0.45	0.47

Slide-Area	m8-c-a2-b	m8-c-a2-b	m8-c-a2-b	o4-a1	o4-a1	o4-a1	o4-a1	o4-a1	old-6b-a2	OLD-6-c
Point #	12	14	20	1	3	5	8	10	11	3
SiO2	24.14	23.77	23.59	25.01	24.45	25.06	24.41	23.88	23.94	24.58
Al2O3	22.75	21.90	21.06	22.11	22.27	22.07	22.84	21.96	22.05	22.57
Cr2O3	0.00	0.00	0.00	0.02	0.02	0.01	0.01	0.01	0.01	0.06
FeO	28.42	27.72	27.98	27.17	27.51	27.35	27.48	26.98	28.83	29.30
MgO	12.44	12.48	12.74	13.72	12.96	13.72	13.07	13.42	12.55	12.47
CaO	0.00	0.00	0.00	0.00	0.01	0.01	0.02	0.05	0.00	0.04
Na2O	0.00	0.00	0.00	0.00	0.00	0.00	0.00	0.00	0.00	0.00
K2O	0.00	0.00	0.00	0.03	0.05	0.03	0.05	0.03	0.06	0.05
TiO2	0.00	0.00	0.00	0.07	0.07	0.09	0.06	0.08	0.11	0.13
MnO	0.24	0.24	0.20	0.28	0.26	0.20	0.26	0.23	0.27	0.27
Total	87.99	86.11	85.58	88.43	87.62	88.55	88.22	86.64	87.81	89.47
					Cations corrected to 28 Oxygens					
Si	5.16	5.19	5.20	5.28	5.22	5.28	5.18	5.16	5.15	5.19
Ti	0.00	0.00	0.00	0.01	0.01	0.01	0.01	0.01	0.02	0.02
Al	5.73	5.63	5.47	5.50	5.61	5.49	5.71	5.59	5.59	5.61
Fe	5.08	5.06	5.16	4.79	4.92	4.82	4.87	4.88	5.19	5.17
Mn	0.04	0.04	0.04	0.05	0.05	0.04	0.05	0.04	0.05	0.05
Mg	3.96	4.06	4.19	4.31	4.13	4.31	4.13	4.32	4.03	3.92
K	0.00	0.00	0.00	0.01	0.01	0.01	0.01	0.01	0.02	0.01
Cation Total	19.98	19.99	20.06	19.96	19.96	19.96	19.97	20.03	20.04	19.99
Xfe	0.56	0.55	0.55	0.53	0.54	0.53	0.54	0.53	0.56	0.57
XMg	0.44	0.45	0.45	0.47	0.46	0.47	0.46	0.47	0.44	0.43

Slide-Area	OLD-6-c	OLD-6-c	OLD-6-c	OLD-6-c-b	OLD-6-c-b
Point #	9	12	14	1	5
SiO2	24.53	24.84	24.68	24.20	25.18
Al2O3	22.55	22.12	21.92	22.49	21.36
Cr2O3	0.06	0.06	0.08	0.08	0.06
FeO	28.42	28.54	28.93	29.11	28.66
MgO	12.26	12.60	12.21	12.19	12.70
CaO	0.01	0.03	0.02	0.03	0.04
Na2O	0.00	0.00	0.00	0.03	0.00
K2O	0.07	0.03	0.05	0.08	0.04
TiO2	0.10	0.10	0.15	0.13	0.11
MnO	0.26	0.28	0.29	0.29	0.28
Total	88.28	88.60	88.33	88.63	88.42
		Cations corrected to 28 Oxygens			
Si	5.22	5.27	5.27	5.16	5.36
Ti	0.02	0.02	0.03	0.02	0.02
Al	5.66	5.53	5.52	5.65	5.36
Fe	5.06	5.07	5.17	5.19	5.10
Mn	0.05	0.05	0.05	0.05	0.05
Mg	3.89	3.99	3.88	3.88	4.03
K	0.02	0.01	0.01	0.02	0.01
Cation Total	19.94	19.95	19.95	20.01	19.94
Xfe	0.57	0.56	0.57	0.57	0.56
XMg	0.43	0.44	0.43	0.43	0.44

Table A.4: Plagioclase

Slide-Area	m8-c-a3-b	m8-c-a2-a	m8-c-a2-b	old-6b-a2	old-6b-a2	old-6b-a2-b	old-6b-a2-b	ml-51a-a	ml-51a-a-b	ml-51a-a-b
Point #	13	9	17	3	9	5	8	4	4	5
SiO2	68.14	67.67	67.30	67.97	66.32	66.57	68.14	59.51	58.92	62.01
Al2O3	20.02	20.12	19.99	20.52	20.15	19.82	20.31	25.16	25.74	24.31
Cr2O3	0	0	0	0	0	0	0	0	0	0
FeO	0.13	0	0	0.31	0.05	0.05	0.04	0.17	0.72	0.06
MgO	0	0	0	0	0	0	0	0	0.28	0
CaO	0.06	0	0	0.24	0.26	0.16	0.08	6.34	6.43	4.87
Na2O	11.45	11.54	11.57	11.60	11.50	11.65	11.76	8.03	7.96	9.05
K2O	0.01	0.00	0	0.09	0.09	0.07	0.07	0.23	0.62	0.15
TiO2	0	0	0	0	0	0	0	0.04	0.08	0.01
MnO	0	0	0	0	0	0	0	0.02	0.03	0
Total	99.92	99.33	98.87	100.72	98.37	98.32	100.40	99.49	100.78	100.45
Cations corrected to 8 Oxygens										
Si	2.98	2.97	2.97	2.95	2.95	2.96	2.97	2.67	2.63	2.74
Al	1.03	1.04	1.04	1.05	1.06	1.04	1.04	1.33	1.35	1.27
Ca	0.00	0.00	0.00	0.01	0.01	0.01	0.00	0.30	0.31	0.23
Na	0.97	0.98	0.99	0.98	0.99	1.00	0.99	0.70	6.88	0.77
K	0.01	0.00	0.00	0.00	0.01	0.00	0.00	0.06	0.04	0.01
Cation Total	4.99	5.00	5.00	5.01	5.02	5.02	5.01	5.02	5.06	5.02
Mol% Anorthite	0.25	0.00	0.00	1.13	1.19	0.79	0.40	28.78	4.25	22.75
Mol% Albite	99.10	100.00	99.92	98.39	98.26	98.82	99.20	65.86	95.26	76.46

Mol% Anorthite = Ca/(Ca+Na+K)*100%; Mol% Albite = Na/(Ca+Na+K)*100%

Slide-Area	ml-51a-a-b	ml-51a-a-b	OLD-6-c	OLD-6-c	ML-50-a	ML-50-a	ML-50-a
Point #	7	8	1	11	6	7	9
SiO2	57.94	61.74	64.16	67.82	60.91	62.47	63.32
Al2O3	26.53	19.18	18.57	19.67	23.92	23.24	22.67
Cr2O3	0	0	0	0	0	0	0
FeO	0.07	0.14	0.05	0.07	0.00	0.07	0.00
MgO	0	0	0	0	0	0	0
CaO	7.51	0.04	0	0	5.12	3.95	3.41
Na2O	7.28	0.66	0.07	11.71	8.63	9.16	9.61
K2O	10.37	14.98	16.25	0.09	0.05	0.13	0.18
TiO2	0.01	0.12	0	0	0	0	0
MnO	0	0.02	0.02	0	0	0	0
Total	99.57	96.90	99.12	99.37	98.63	99.03	99.19
Cations corrected to 8 Oxygens							
Si	2.60	2.94	2.99	2.98	2.74	2.79	2.82
Al	1.40	1.08	1.02	1.02	1.27	1.22	1.19
Ca	0.36	0.00	0.00	0.00	0.25	0.19	0.16
Na	0.63	0.06	0.01	1.00	0.75	0.79	0.83
K	0.01	0.91	0.97	0.00	0.00	0.01	0.01
Cation Total	5.02	5.00	4.99	5.01	5.01	5.00	5.01
Mol% Anorthite	35.77	0.25	0.00	0.00	24.60	19.09	16.20
Mol% Albite	62.89	6.24	0.66	99.52	75.08	80.18	82.76

Mol% Anorthite = Ca/(Ca+Na+K)*100%; Mol% Albite = Na/(Ca+Na+K)*100%

Table A.5: Fe-sulphides

Slide-Area	O3-A	O3-A	O3-A	O3-A	ML_51B	ML_51B	ML_51B	ML_51B	ML_51B	ML_51B
Point #	2	4	5	6	1	3	6	8	10	12
Mineral	Arsenopyrite	Arsenopyrite	Arsenopyrite	Arsenopyrite	Arsenopyrite	Arsenopyrite	Arsenopyrite	Arsenopyrite	Arsenopyrite	Arsenopyrite
S	21.31	20.25	20.70	20.52	20.78	21.08	21.39	20.92	20.82	21.10
Fe	34.44	34.01	34.39	33.84	34.27	34.45	35.21	34.39	34.69	34.78
As	45.01	46.46	45.82	46.79	45.90	45.60	45.57	46.20	45.99	45.92
Au	0.10	0.10	0.03	0.06	0.03	0.09	0.09	0.07	0.05	0.05
Zn	0.13	0.14	0.09	0.12	0.17	0.14	0.09	0.13	0.11	0.12
Pb	0.23	0.19	0.19	0.20	0.20	0.23	0.22	0.21	0.21	0.20
Cu	0.04	0.06	0.07	0.08	0.08	0.07	0.09	0.03	0.09	0.06
Total	101.25	101.22	101.28	101.63	101.43	101.65	102.66	101.95	101.95	102.24

Slide-Area	ML_51B	ML_51B	ML_51B	ML_51B	ML_51B	ML_51B	ML_51B	ML_51B	ML_51B-b	O3-A
Point #	13	14	2	4	5	7	9	11	6	3
Mineral	Arsenopyrite	Arsenopyrite	Phyrrhotite	Pyrrhotite	Pyrrhotite	Pyrrhotite	Pyrrhotite	Pyrrhotite	Pyrrhotite	Pyrite
S	20.79	21.28	39.39	39.64	39.58	39.78	39.30	39.90	39.57	54.47
Fe	34.31	34.76	60.85	61.57	61.16	61.03	61.35	61.01	61.01	47.60
As	45.89	45.57	0.06	0	0	0	0	0	0	0
Au	0.00	0.03	0.04	0.05	0.05	0.08	0.08	0.05	0.06	0.04
Zn	0.15	0.08	0	0	0	0	0	0	0	0
Pb	0.21	0.21	0.41	0.41	0.41	0.38	0.41	0.42	0.41	0.54
Cu	0.11	0.08	0	0	0	0	0.04	0	0	0
Total	101.47	102.01	100.74	101.67	101.19	101.27	101.17	101.38	101.05	102.65

Slide-Area	O3-A	O3-A
Point #	1	7
Mineral	Chalcopyrite	Chalcopyrite
S	35.51	36.44
Fe	30.47	30.35
As	0	0
Au	0.01	0.05
Zn	0.11	0.04
Pb	0.35	0.35
Cu	34.03	33.43
Total	100.48	100.66

Table A.6: Fe-oxides

Slide-Area	Car-A	Car-A	Car-A
Point #	1	2	3
Mineral	Ilmenite	Rutile	Rutile
SiO2	0.06	0.54	0.02
Al2O3	0.06	0.25	0.05
Cr2O3	0.18	0.11	0.05
FeO	46.62	0.85	0.22
MgO	0.03	0	0.01
CaO	0.08	0.05	0.07
Na2O	0	0.02	0
K2O	0.11	0.14	0.10
TiO2	52.50	94.90	99.58
MnO	0.37	0.07	0.07
Total	100.01	96.95	100.19

Slide-Area	ML_51B-b	ML_51B-b	ML_51B-b	ML_51B-b	ML_51B-b	ML_51B-b
Point #	1	2	3	4	5	7
Mineral	Oxide	Oxide	Oxide	Oxide	Oxide	Oxide
S	0	0	0	0.02	0	0
Fe	26.45	26.26	26.67	26.78	25.59	20.08
As	0	0	0	0	0	0
Au	0	0	0	0	0	0
Zn	0	0	0	0	0	0
Pb	0	0	0	0	0	0
Cu	0	0	0	0	0	0
Total	26.45	26.26	26.67	26.81	25.59	20.08

This slide was tested with sulphide parameters because these points were believed to be sulphides prior to microprobe analysis.

Sample number given in upper left corner, microprobe sample points labeled on pictures.
Point analysis contained in Appendix A.

O1-B-1

JEOL COMP   15.0kV   ×40   100µm WD11mm

O1-B-A2

JEOL COMP   15.0kV   ×150   100µm WD11mm

O1-B-A3

15-bio
16-chl 14-ilmenite
17-muscl
13-bio
12-cal
2-mus 1-bio
18-chl
3-mus
9-Clz
5-cal
6-chl
7-mus
4-cal
11-bio
10-chl 5-Fe-ox

JEOL COMP 15.0kV ×150 100μm WD11mm

O1-B-A4

10-mus
9-?
8-bio
1-clz
2-cal
3-bio
7-chl
6-mus
5-chl
4-clz?

JEOL COMP 15.0kV ×150 100μm WD11mm

82

OLD_6B_A2

1-FeS
2-Qtz
3-Plag
4-Musc
5-Qtz
6-Bio
7-Chl
8-Musc
10-Bio
11-Chl
9-Plag

JEOL COMP 15.0kV ×100 100μm WD11mm

OLD_6B_A2

5-Plag
3-Qtz
4-Qtz
10-Bio
2-Bio
1-Musc
8-Plag
9-Qtz
7-Bio
6-Cal

JEOL COMP 15.0kV ×100 100μm WD11mm

Old_6

6-Ilm
10-Bio
9-Qtz
7-Cal
1-Chl
4-Cal
2-Qtz
18-Chl
5-Chl
8-Fe-ox

JEOL COMP 15.0kV   ×150   100µm WD11mm

Old_6

7-Musc 8-Qtz   9-Chl
10-Cal
2-Qtz
11-Plag
1-Musc
6-N/A
3-Chl
13-Musc   4-Bio
12-Chl
14-Chl
5-Qtz

JEOL COMP 15.0kV   ×100   100µm WD11mm

Car-A

JEOL COMP   15.0kV   ×40   100µm WD11mm

ML-51B-b

JEOL COMP   15.0kV   ×40   100µm WD11mm

ML-51B

1-Aspy 2-Po
3-Aspy
4-Po
5-Po
8-Aspy
6-Aspy
7-Po

JEOL COMP   15.0kV   ×40   100µm WD11mm

ML-51B

9-Po
13-Aspy
12-Aspy
11-Po
10-Aspy
14-Aspy

JEOL COMP   15.0kV   ×40   100µm WD11mm

O3-A

4-Aspy   3-Py

1-Chpy

2-Aspy

JEOL COMP   15.0kV   ×40   100μm WD11mm

O3-A

5-Aspy

6-Aspy

7-Chpy

JEOL SEI   15.0kV   ×40   100μm WD11mm